2017

Study of the photoluminescence spectra of Mg-doped GaN

Puranjan Ghimire
Virginia Commonwealth University

Study of the photoluminescence spectra of Mg-doped GaN

A thesis submitted in partial fulfillment of the requirements for the degree of Master of Science in Physics and Applied Physics at Virginia Commonwealth University.

by

Puranjan Ghimire

B.Sc. Physics, Tribhuvan University, 2009

Director:

Dr. Michael A. Reshchikov

Professor, Department of Physics

Virginia Commonwealth University

Richmond, Virginia

Summer, 2017

Acknowledgements

My utmost gratitude goes to Dr. Michael Reshchikov for his continuous motivation towards my work. He is the first man behind my success. I will be indebted to Dr. Reshchikov for the rest of my life for teaching me the rule of success; continuous hard work.

My utmost gratitude also goes to my friend Cara M. Frame who helped me in every problem, be it in academia or in life. She is the reason I survived in VCU. Cara, you are the person with a heart of gold. I am very grateful to my fate that led me to VCU to meet a great human like you.

I would like to thank Dr. Marilyn F. Bishop who taught me the physical meaning of complex equations. I will always remember Dr. Bishop for her time and effort to make me understand the homework problems in a much-simplified way.

A load of thanks goes to my friends/brothers Dinesh Bista, Vikash Chauhan, Anjan Pradhan, Diwakar Pudasaini, Maksudul Rana, Swopnil Parajuli, Pranav Panta, Janakiram Reddy, Vishal Shah, Michael, Nahla and countless others. I will always remember the time that I spent with you. Your support and motivation in the time of need played a crucial role for who I am now.

I would also like to thank my parents, my brother-Ranjan, my sister- Sujan, my brother in-law-Sujan subedi for their immense love, support and best wishes towards me.

I would like to thank the faculty and staff of physics department for providing a conducive atmosphere for study and research.

Finally, I would also like to appreciate the partial support from NSF (grant DMR-1410125).

Table of Contents

List of Figures v

Abstract viii

1. Introduction 1

1.1 Motivation 1
1.2 GaN Semiconductor 2
2. Literature review 4

2.1 Mg-doped GaN 4
2.2 Potential fluctuations model 5
2.3 Donor acceptor pair model 8
2.4 Abrupt and tunable thermal quenching of PL in GaN 11
2.5 Phenomenological model of the abrupt and tunable thermal quenching 14
3. Experimental Details 20

3.1 Sample 20
3.2 Experimental set-up 20
4. Results and Discussion 25

4.1 PL spectra 25
4.2 Deconvolution of PL spectra 32
4.3 Dependence on Excitation intensity: 46
a) Potential fluctuation model: 47
b) Donor Acceptor Pair model: 49
4.4 Dependence on temperature 56
i) PL Intensity 56
a) Temperature dependence of the exciton peak intensity 58
b) Temperature dependence of the UVL peak intensity 59
c) Temperature dependence of the BL* peak intensity 60
II) BL* band peak position 65
5. Conclusions 81

References 85

List of Figures

Figure 1.2-1: Wurtzite crystal structure (on the left) and zinc-blende crystal structure (on the right) of GaN. 3

Figure 2.2-1: Schematic band diagram and defect levels showing potential fluctuations under conditions of PL. 16

Figure 2.3-1: PL band positions (ZPL) as a function of excitation intensity. 17

Figure 2.4-1: Evolution of the PL spectrum in p-type Mg-doped GaN with increasing temperature from 20 to 200 K with step 20 K. 18

Figure 2.4-2: Temperature dependence of quantum efficiency of the UVL band in p-type Mg-doped GaN for different $\mathrm{P_{exc}}'\mathrm{s}$. 19

Figure 3.2-1: Experimental set up for PL measurements. 23

Figure 3.2-2: Detailed schematics of a monochromator. 24

Figure 3.2-3: Simplified view of a photomultiplier tube. 24

Figure 4.1-1: PL spectra at different excitation intensities. 28

Figure 4.1-2: PL spectra at various temperatures but fixed excitation intensity. 29-31

Figure 4.2-1 (a): PL spectrum (at $\mathrm{P_{exc}} = 0.2\ \mathrm{W/cm^2}$) and model UVL at $\mathrm{T} = 13.5\ \mathrm{K}$. ... 36

Figure 4.2-1 (b): PL spectrum (at $\mathrm{P_{exc}} = 0.2\ \mathrm{W/cm^2}$) and model UVL at $\mathrm{T} = 140\ \mathrm{K}$. ... 36

Figure 4.2-1 (c): PL spectrum (at $\mathrm{P_{exc}} = 2.9\times10^{-5}\ \mathrm{W/cm^2}$) and model UVL at $\mathrm{T} = 110\ \mathrm{K}$. 37

Figure 4.2-2 (a): Deconvoluted PL spectrum at $T = 13.5\ K$ and $P_{exc} = 0.2\ W/cm^2$ 38

Figure 4.2-2 (b): Deconvoluted PL spectrum at $T = 140\ K$ and $P_{exc} = 0.2\ W/cm^2$ 39

Figure 4.2-2 (c): Deconvoluted PL spectrum at $T = 110\ K$ and 40

Figure 4.2-3: Magnified view of main peak area of model UVL and UVL band of PL spectra of Fig 4.2-1 (a) 41

Figure 4.2-4 (a): Deconvoluted BL band corresponding to Fig. 4.2-2 (a). 42

Figure 4.2-4 (b): Deconvoluted BL band from Fig. 4.2-2 (b)..... 43

Figure 4.2-4 (c): Deconvoluted BL band from Fig. 4.2-4 (c). 44

Figure 4.2-5: Fits to the deconvoluted blue bands using Eq. (4.2-1) at various excitation intensities and $T = 13.5\ K$. 45

Figure 4.3-1: Peak positions of BL, UVL and exciton band with respect to excitation intensities. 55

Figure 4.4-1: Temperature dependence of the peak intensity of various bands..... 67-69

Figure 4.4-2: Temperature dependence of BL peak intensity measured at different days for fixed excitation intensity. 70-72

Figure 4.4-3: Temperature dependence of the UVL peak intensity measured at different days for fixed excitation intensity. 73-75

Figure 4.4-4: Dependence of characteristic temperature T_0 on generation rate for the PL bands: 76-77

Figure 4.4-5: Temperature dependence of the BL^* band..... 78

Figure 4.4-6: Energy band diagrams for (a) n-type and (b) p-type GaN. 78

Figure 4.4-7: Dependence of inverse of characteristic temperature (T_0) of quenching and critical temperature (T^*) of the shift of the BL^* band on generation rate (G) for $P_{exc} \leq 0.0002\,W/cm^2$. 79

Figure 4.4-8: Calculated dependence of PL quantum efficiency and concentration of electrons and holes in the conduction and valence bands respectively ……...80

Abstract

Study of the photoluminescence spectra of Mg-doped GaN

By Puranjan Ghimire, MS

A Thesis submitted in partial fulfillment of the requirements for the degree of Master of Science in Physics and Applied Physics at Virginia Commonwealth University.

Virginia Commonwealth University, 2017

Director:
Dr. Michael A. Reshchikov
Professor, Department of Physics

We have studied luminescence properties of Mg-doped GaN grown by hydride vapor phase epitaxy. Steady state photoluminescence (PL) spectra have been analyzed.

Exciton, ultraviolet luminescence (UVL) and blue luminescence (BL) bands are the dominant PL bands in the spectra. At low temperature, Exciton and UVL bands show almost no shift with excitation intensity, whereas the BL band blueshifts by almost 0.4 eV with increasing excitation intensity by seven orders of magnitude. Such shifting nature of bands with excitation intensity is explained by assuming that the BL band is detected from the region of the sample where potential fluctuations are very large, but the UVL and exciton bands originate from the region of the sample where there are no potential fluctuations. After the careful analysis of potential fluctuations model and the donor-acceptor pair model, we conclude that the BL band in the studied GaN:Mg sample is not a separate band but the UVL band itself, which is significantly distorted by potential fluctuations. Now, we call this band the BL* band. Temperature dependence of the BL*, UVL and Exciton peak intensity is analyzed. We see abrupt and tunable thermal quenching of the BL* and Exciton bands. Temperature dependence of the BL* and UVL bands at fixed excitation intensities but at different environmental conditions is also investigated. Finally, giant redshift of the BL* band with increasing temperature is explained by a combination of potential fluctuations and abrupt quenching of the BL* band with temperature.

1. Introduction

1.1 Motivation

Converting electricity into light was perhaps one of the most significant inventions of human intellect. Since the invention of first light bulb, scientists and engineers have been constantly trying to increase the efficiency, reduce the cost and energy consumption of the lighting devices. Gallium Nitride (GaN) has drawn attraction of physicists and engineers because of its wide bandwidth and chemical and structural stability that withstand high voltage, high heat, and radiation. Today, GaN is a basic material for bright white and blue light emitting diodes (LED) and blue lasers. Moreover, new kinds of nanotubes, microwave radio frequency power amplifiers, solar cells, and transistors are among new applications of GaN. Gallium Nitride semiconductor is superior to other semiconductors in many aspects. In particular, it has a very high electrical resistance which allows it to handle over ten times more voltage than silicon before electrical breakdown.

Despite the wide use of GaN in varieties of devices, highly efficient and reliable devices based on GaN can be achieved only when one understands the origin and properties of defects that are present in GaN intentionally and unintentionally doped. Among the techniques used to analyze the optical and electrical properties of GaN, photoluminescence (PL) is the leading one, especially for GaN, because of its wide and direct band gap. Furthermore, PL is a nondestructive method that enables researchers to study luminescence spectrum associated with defects. With the thorough analysis of

spectra, one can get the type, energy levels and concentration of point defects in a sample. This information will be of great importance to enhance the performance of devices based on GaN material.

PL technique has many benefits. Luminescence spectra obtained at different temperatures and excitation intensities contain information which if deciphered can render deep insight about the defects present in the sample. Shifts of the band maxima with temperature and excitation intensity, enhancement of some PL bands and thermal quenching of other bands are among common phenomena that we generally see in PL spectra. Two main models that describe shifts of PL bands with excitation intensity are potential fluctuations model and donor acceptor pair (DAP) model. Rate-equations model is used to describe normal and abrupt thermal quenching of PL.

In this thesis, we have analyzed Mg-doped GaN grown by hydride vapor phase epitaxy (HVPE). We have obtained the PL spectra at different temperatures (from $13.5\,K$ to $320\,K$) and various excitation intensities (from $2.8\times10^{-7}W/cm^2$ to $0.2\,W/cm^2$). Peak positions of each band (Exciton, UVL, and Blue) as a function of temperature and excitation intensity have been analyzed. Peak intensity vs temperature has also been studied. Abrupt thermal quenching is observed at comparatively low excitation intensities.

1.2 GaN Semiconductor

Gallium Nitride (GaN) is a binary III/V binary direct band-gap semiconductor available in two crystal structures. Wurtzite crystal structure (Fig.1.2-1) is the stable one. The other crystal structure which GaN assumes is Zinc-blende crystal structure (Fig.1.2-1) which

is metastable. The band gap of GaN depends on the crystal structure. In particular, the band gap of wurtzite crystal structure is $3.43\,eV$ at $300\,K$ and $3.50\,eV\ at\ 2K$. The wurtzite crystal structure is an example of hexagonal crystal system. GaN is generally grown by molecular beam epitaxy (MBE), metal organic chemical vapor deposition (MOCVD) and hydride vapor phase epitaxy (HVPE). Silicon (Si), Oxygen (O) and Germanium (Ge) are commonly used dopants to make n-type GaN. Magnesium (Mg) is the only impurity which is used to make p-type GaN.

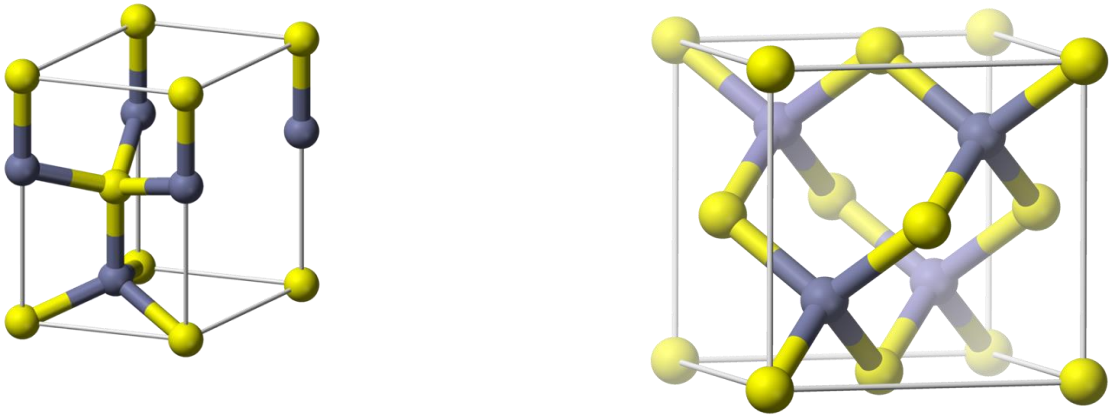

Fig. 1.2-1: Wurtzite crystal structure (on the left) and zinc-blende crystal structure (on the right) of GaN.

(https://en.wikipedia.org/wiki/File:Wurtzite-unit-cell-3D-balls.png

https://en.wikipedia.org/wiki/File:Sphalerite-unit-cell-depth-fade-3D-balls.png*)*

2. Literature review

2.1 Mg-doped GaN

Magnesium is the most important impurity in GaN because Mg-doping enables one to achieve reproducible p-type GaN. It is well established that doping with Mg introduces the shallow acceptor Mg_{Ga} with an ionization energy of $\sim 200\ meV$.[16] Some experimental results were explained in an assumption that Mg doping introduces optically active deep acceptors.[1] However, these assumptions are not verified by further experiments. Rather, compensating deep donors are formed at high doping levels that affect the optical properties of GaN:Mg.[2] The origin of these compensating deep donors is yet a topic of debate.

Useful information on p-type GaN such as material properties, defect formation, etc., can be obtained by the study of optical emission in Mg-doped GaN. PL from low and moderately doped GaN:Mg shows a strong enhancement of the ultraviolet luminescence (UVL) band with a relatively sharp peak at about 3.26 eV followed by a few LO phonon replicas.[3] With the increase in the concentration of Mg-doping, the peaks of the UVL band broaden, redshift, and transform into a single structureless band with a maximum at about $3.2\ eV$.[4,5] At Mg concentration above $10^{19}\ cm^{-3}$, a broad blue luminescence (BL) band with a maximum at about $2.7 - 2.9\ eV$ appears which generally dominates the PL spectrum of heavily doped GaN.[4] The BL band is attributed to the transition between a deep donor and the Mg_{Ga} acceptor. The donor acceptor pair (DAP) emission energy depends on the pair separation due to Coulomb interaction between

ionized centers in the final state of recombination. The detailed discussion on DAP transition will be presented in section 2.3.

With the emergence of the BL band as a dominant transition, the hole concentration saturates and decreases with further Mg concentration, indicating a self-compensating process.[4,5] Several researchers have noted that in highly compensated or heavily doped semiconductors, there exist high potential fluctuations which might play a crucial role in band broadening, shifting etc. with the variation of temperature and excitation intensity.[4,6] In highly compensated or heavily doped semiconductors, random distribution of charged impurities, e.g. donors and acceptors, gives rise to potential fluctuations.[7] The potential fluctuations are screened by free electrons in n-type GaN. However, high potential fluctuations may exist in highly compensated Mg-doped GaN especially at low temperature because of the absence of screening effect as the very insignificant number of equilibrium holes are present. Hence, in heavily doped GaN, an account for potential fluctuations is crucial to get a deep insight on defects and defect related PL bands.

2.2 Potential fluctuations model

The potential fluctuations which arise due to inhomogeneous distribution of charged defects play a significant role in the optical properties of compensated or highly doped semiconductors. Potential fluctuations facilitate diagonal transitions with reduced energy as shown in Fig. 2.2-1. This leads to a shift of the PL bands to lower photon energy. The typical amplitude of potential fluctuations γ and average radius r_s of unscreened potential in a highly compensated p-type semiconductor are given as[7]

$$\gamma = \frac{e^2}{4\pi\epsilon_0\epsilon}\frac{{N_t}^{2/3}}{p^{1/3}} \tag{2.2-1}$$

and

$$r_s = {N_t}^{1/3}p^{-1/3}, \tag{2.2-2}$$

where, $N_t = {N_A}^- + {N_D}^+$ is the total concentration of charged donors and acceptors and p is the concentration of free holes. The other parameters have their usual meaning.

The fluctuation amplitude at a very low degree of compensation is given by

$$\gamma = 0.26\frac{e^2}{4\pi\epsilon_0\epsilon}\left(\frac{4\pi}{3}N_A\right)^{1/3}\left(\frac{N_D}{N_A}\right)^{1/4}. \tag{2.2-3}$$

The screening radius for this case is

$$r_s = 0.58{N_D}^{-1/2}{N_A}^{1/6}. \tag{2.2-4}$$

Comparison of equations (2.2-1) and (2.2-3) shows that potential fluctuations are greater for the material which has a higher concentration of ionized defects and a higher degree of compensation. It may be expected that amplitude of potential fluctuations lies between the limiting values for very high and very low degree of compensations. It is clear from equation (2.2-1) that fluctuations increase with a decrease in excitation intensity but its amplitude is limited by the width of the band gap.

The photon energy ($\hbar\omega$) which corresponds to zero phonon line (ZPL) in the case of DAP transition when potential fluctuations are present is given as[8,9]

$$\hbar\omega = E_g - (E_D + E_A) - 2\gamma, \tag{2.2-5}$$

where E_g is the band gap energy, E_D and E_A are ionization energies of donor and acceptor and γ is the amplitude of fluctuations which is calculated using equations (2.2-1) or (2.2-3). We ignored the Coulomb interaction term in Eq. (2.2-5) for simplicity. In the case of band-to-band transitions, the terms in the parenthesis of equation (2.2-5) should be removed and in the case of eA transition, E_D term is removed. For example, for band-to-band transition, equation (2.2-5) becomes [10]

$$\hbar\omega = E_g - 2\gamma. \tag{2.2-6}$$

While obtaining equations (2.2-5) and (2.2-6), it is considered that the photogenerated electrons and holes move quickly to the potential minima and maxima of the conduction and valence band respectively after excitation (Fig. 2.2-1). Then they recombine with a certain probability which is determined by the degree of overlap of recombining carriers. If it is DAP transition, electrons and holes are first captured by donor and acceptor, respectively. In either case, i.e. band-to-band transition or DAP transition, there will be a spatial separation between recombining carriers which results in diagonal transitions reducing the emission energy (see Fig. 2.2-1).

As discussed above, free carriers first come to potential wells and then are captured by defects and recombine. Electrons and holes inside such wells and hills are localized. Therefore, each well and hill can be considered as a point defect. Hence, transitions that happen in heavily doped or compensated semiconductors have many similar features with DAP-type transitions. For example, PL bands in both cases (i.e., DAP type or the one influenced by potential fluctuations) blueshift with increase in excitation intensity. However, the reason behind the blueshift in the case of DAP type

transition is different. The more detailed explanation of DAP model is given in the Sec. 2.3.

2.3 Donor acceptor pair model

DAP model allows us to find emission energy for the transition between donor and acceptor. It takes into account the Coulomb interaction between charged donor and acceptor while giving the expression for photon energy emitted as a result of DAP recombination. According to this model, for distant DAP, the dependence of the zero-phonon line ($\hbar\omega$) on the pair separation (R) is given by [11]

$$\hbar\omega = E_g - (E_D + E_A) + \frac{q^2}{4\pi\epsilon_0\epsilon R}\,, \tag{2.3-1}$$

where ϵ is the low-frequency dielectric constant and q is the electron charge. E_D and E_A are donor and acceptor energy when there is no Coulomb interaction or, in other words, when donor and acceptor pair are infinitely far from each other. The last term represents the Coulomb energy resulting from the interaction of ionized donor and acceptor pair. This model suggests that the PL band has the lowest energy at low excitation intensity because the most distant pairs contribute to the PL spectrum. The transition between distant pairs is comparatively slow because carriers' wavefunction has smaller overlap. This leads to the earlier saturation of PL originating from distant pairs with increasing excitation intensity. Therefore, PL band shifts to higher photon energy with increasing excitation intensity as the closest pairs contribute more to the PL spectrum.

For DAP model, Zacks and Halperin[12] developed a theoretical relation between the photon energy ($\hbar\omega$) corresponding to ZPL and the excitation intensity (P_{exc}) assuming that one of the defects has much larger wavefunction than another as

$$P_{exc} = D\frac{(\hbar\omega-\hbar\omega_\infty)^3}{\hbar\omega_B+\hbar\omega_\infty-2\hbar\omega}e^{\left(-2\frac{(\hbar\omega_B-\hbar\omega_\infty)}{\hbar\omega-\hbar\omega_\infty}\right)}, \quad (2.3\text{-}2)$$

where D is a proportionality factor, $\hbar\omega_\infty$ is the emission energy corresponding to ZPL when components of DAP are infinitely far from each other (i.e., no Coulomb interaction between them) and $\hbar\omega_B$ is defined as $\hbar\omega_B = E_B + \hbar\omega_\infty$ with $E_B = \frac{e^2}{4\pi\epsilon_0\epsilon R_B}$, R_B being the largest Bohr radius (it can be either of donor or acceptor) and ϵ being the low-frequency dielectric constant ($\epsilon = 9.5$ for GaN).

Unlike the transitions between carriers (free or bound) that are localized by potential fluctuations, the shift of the PL band in DAP case is due to the saturation of the PL emission from distant pairs. In the former case, the shifting of the band to higher energy with increasing excitation intensity is explained by the fact that transitions become more vertical (Fig. 2.2-1) because of screening of the potential fluctuations by photogenerated carriers. In the latter case, the PL emission from distant pairs has longer life-time because of the smaller overlap of the wavefunctions than for the relatively close pairs. The transitions between relatively close pairs contribute to the emission at greater photon energy than between the distant pairs because of the Coulomb energy term in equation (2.3-1) which is bigger for close pairs than for distant pairs.

The difference between potential fluctuations model and DAP model can be understood more profoundly if we analyze equations (2.2-5) and (2.3-1). Fluctuation amplitude (γ) in equation (2.2-5) increases with the decrease in excitation intensity but the Coulomb interaction energy term in (2.3-1) increases with the increase in excitation intensity as relatively close pairs contribute to the PL emission due to the saturation of distant pairs. The reason why in both cases emission energy increases with increasing excitation intensity is because of the negative sign of fluctuation amplitude (γ) in equation (2.2-5) and the positive sign of Coulomb interaction energy term in equation (2.3-1). This indicates that the shift of PL band in the case of DAP emission saturates at limiting value of low excitation intensity (i.e., infinitely distant pairs contribute to the PL emission and there will be no Coulomb interaction) and also saturates at the limiting value of high excitation intensity (i.e., closer pairs contribute to the PL emission and Coulomb interaction is so large that defect levels approach the conduction or valence band). However, in the case of potential fluctuations, the shift in the PL band saturates only in the limiting case of high excitation intensities where there are no fluctuations due to screening effects by excess photogenerated carriers. Another significant difference between DAP model and the potential fluctuations model is the following. The undistorted positions of defect levels correspond to the limit of low excitation intensity (i.e, Coulomb interaction tends to zero) in the case of DAP model but the ideal positions of defect levels correspond to the limit of high excitation intensity (i.e., potential fluctuations vanish) in the case of potential fluctuations model.

The difference between DAP model and potential fluctuations model can be better understood by Fig. 2.3-1 which shows the PL band position as a function of

excitation intensity. The figure contains three curves. First one is the “Ideal case” which assumes that there are no potential fluctuations in the sample and no Coulomb interactions between charged donors and acceptors. Second is the “Potential Fluctuation model”. Band position in the case of “Potential Fluctuation model” approaches the “Ideal case” when excitation intensity is high, indicating that fluctuations tend to vanish. But the band position decreases when excitation intensity decreases, which shows that fluctuations increase with decreasing excitation intensity. In the case of “DAP model”, the band position approaches the “Ideal case” when excitation intensity decreases, indicating that Coulomb interaction is tending to zero. As excitation intensity increases, band position tends to saturate indicating that Coulomb interaction is maximum.

2.4 Abrupt and tunable thermal quenching of PL in GaN

In the recent studies on high-resistivity Zn-doped GaN, p-type Mg-doped GaN and high resistivity undoped GaN, abrupt thermal quenching of PL bands was observed.[13,14,15] In Zn-doped GaN, the intensity of the blue luminescence band which is attributed to transitions from a shallow donor (at low temperature) or from the conduction band (at elevated temperature) to the Zn_{Ga} acceptor,[16] dropped by more than two orders of magnitude within a small range ($\sim 10\ K$) of temperatures.[13] The UVL band in some samples of Mg-doped GaN dropped by almost three orders of magnitude within the temperature range of $100 - 180\ K$.[14] Likewise, the UVL band in high-resistivity undoped GaN dropped by two and a half orders of magnitude within a temperature range of

$110 - 130\ K$.[15] In all of the above-mentioned cases, the characteristic temperature (the temperature at which the sudden drop begins) could be tuned by excitation intensity. i.e., the characteristic temperature increased with increasing excitation intensity. Hence, those abrupt quenching were not only abrupt, but also tunable. A detailed review on abrupt thermal quenching of the UVL band in Mg-doped GaN[14] is presented below.

Different PL behavior with temperature was found in different p-type Mg-doped samples. Three MBE grown Mg-doped samples were studied.[14] The UVL band from one of the samples (9600: group A) quenched in the temperature range of $60 - 200\ K$ by an order of magnitude with an activation energy of $30\ meV$. However, the UVL band in other two samples (9591 and 9599: group B) quenched by about four orders of magnitude in the temperature range of $100 - 180\ K$. Evolution of PL spectra on temperature for both groups of samples is shown in Figs. 2.4-1 (a) and (b).

Fig. 2.4-2 (a) shows the dependence of absolute quantum efficiency of the UVL band on temperature. Quantum efficiency (η) is calculated as the ratio of integrated PL intensity (I^{PL}) of a specific band to the electron hole pair generation rate (G) produced by laser per unit volume per second. Mathematically, $\eta = \frac{I^{PL}}{G}$. Quantum efficiency of the UVL band in group B sample (9591), as shown in Fig. 2.4-2 (a), drops abruptly as compared to the group A sample (9600) where the decrease is slow. Characteristic temperature (T_0) at which the quenching occurs increases with increase in excitation intensity for group B samples, whereas, it is nearly constant in group A sample and occurs at a much lower temperature. This can also be seen from Fig. 2.4-2 (b) which

shows the inverse of characteristic temperature as a function of generation rate of electron hole pair (or excitation intensity).

It was postulated that the system must undergo a transition from population inversion of charge carriers in the band gap at $T < T_0$ to a quasi-equilibrium population at $T > T_0$ when abrupt and tunable thermal quenching occurs.[13] The same concept is applied to understanding the abrupt and tunable thermal quenching of the UVL band in group B GaN:Mg samples. The detailed explanation on this will be presented in the Sec. 2.5.

The dependence of the inverse of characteristic temperature on the logarithm of generation rate (Fig. 2.4-2 (b)) is described by the following relation:[13]

$$T_0 = \frac{E_A}{k \ln(B/G)}\,, \tag{2.4-1}$$

with

$$B = C_{pA}(\eta_0{}^{-1} - 1)(N_A - N_D)N_v/2. \tag{2.4-2}$$

Here, E_A is the ionization energy of the acceptor A responsible for the abrupt quenching of PL. k is Boltzmann's constant, C_{pA} is the hole-capture coefficient for the acceptor. η_0 is the internal quantum efficiency of PL via the acceptor A at temperatures below T_0, N_A and N_D are concentrations of the acceptor and shallow donor, respectively, and N_v is the effective density of states in the valence band. The solid line in the Fig. 2.4-2 (b) is the fit with equation (2.4-1). From this fit, ionization energy of the acceptor was obtained to be about $250 - 270\,meV$, which is slightly larger than the ionization energy of the Mg_{Ga} acceptor ($150 - 200\,meV$).[16] The discrepancy between the obtained value and

the reported value is attributed to the potential fluctuations which are prevalent in heavily doped or compensated semiconductors.

2.5 Phenomenological model of the abrupt and tunable thermal quenching

Phenomenological model considers three defect levels to explain the abrupt and tunable thermal quenching of PL.[13] The first defect is a shallow acceptor (Mg_{Ga} in the group B samples explained above). Shallow donor is the second defect which may possibly be O_N or V_NH.[17] The third defect must be included in the model to account for less than 100% quantum efficiency of PL. The third defect is assumed to be an unknown non-radiative deep donor (S).

This model explains that at low temperature ($T < T_0$), the nonradiative centers are filled with electrons in conditions of steady-state PL. This causes the accumulation of electrons in the conduction band as the capture of free electrons by S centers becomes inefficient. Accumulation of electrons in the conduction band results in n-type conductivity, which may reach $10^{16} cm^{-3}$ even at low excitation intensity.[13] At higher temperatures ($T > T_0$), shallow acceptors (Mg_{Ga}) receive enough thermal energy to emit holes to the valence band. The increase in concentration of free holes in the valence band at higher temperatures resumes the p-type conductivity. These free holes in the valence band now efficiently recombine with the electrons at the S centers. The recombination channel via S centers becomes unblocked and the concentration of free electrons abruptly drops. Since most of the recombination now takes place via S

centers, the PL from DAP transitions decreases significantly for $T > T_0$. In a nutshell, the process of quenching begins when holes at the shallow acceptors (Mg_{Ga}) get enough thermal energy to be emitted to the valence band and captured by efficient S centers.

The group A samples explained in above section does not show abrupt and tunable thermal quenching. For group A samples, UVL band is quenched with a very low activation energy in a wide temperature range. The reason behind no abrupt and thermal quenching in group A sample despite it being the Mg-doped sample as samples of group B, is preliminarily attributed to different kinds of nonradiative centers in different samples.[14] More investigation is needed to get a robust conclusion about the different PL behavior in the samples of these two groups.

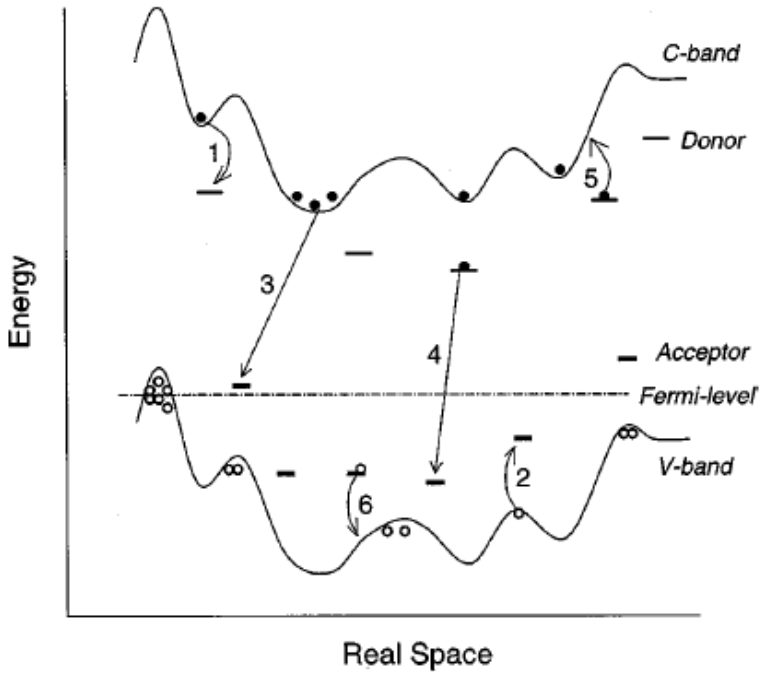

Fig. 2.2-1: Schematic band diagram and defect levels showing potential fluctuations under conditions of PL. Both long-and short-range potential fluctuations are present. Arrows indicate the following transitions: 1, the capture of excess electrons by deep donors; 2, the capture of excess holes by acceptors; 3, radiative recombination of free electrons and bound holes; 4, radiative recombination in DAP; 5, the thermal release of bound electrons to the conduction band; and 6, thermal release of bound holes to the valence band. (Figure and caption are both taken from Ref. 4)

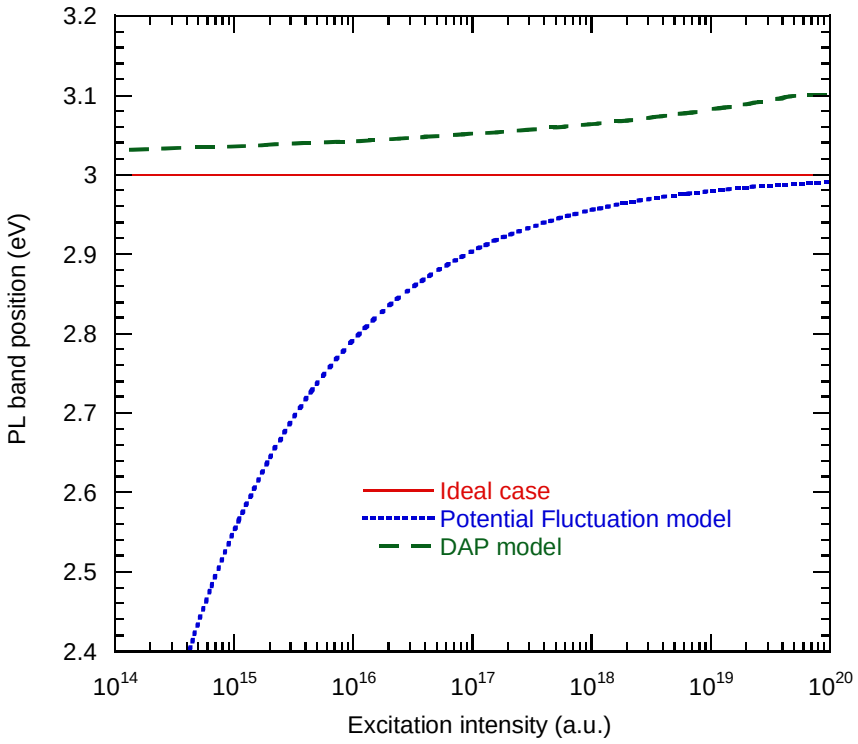

Fig. 2.3-1: PL band positions (ZPL) as a function of excitation intensity. Potential fluctuation model is plotted with equation (2.2-5) with $N_t = 5\times10^{18}$*. Equation 2.3-2 is plotted for DAP model with parameters:* $D = 0.3\times10^{24}$*,* $\hbar\omega_\infty = 3\ eV$ *and* $\hbar\omega_B = 3.2\ eV$*. "Ideal" case is when the band is not affected by potential fluctuations and there is no Coulomb interaction between donors and acceptors. "Ideal" case is plotted for the equation* $\hbar\omega = E_g - (E_d + E_A)$ *which is in fact equations (2.2-5) and (2.3-1) when potential fluctuation (*γ*) and Coulomb interaction tend to zero in the limit of high excitation intensity in the case of Potential fluctuation model and in the limit of low excitation intensity in DAP model.* $E_g = 3.5\ eV, E_d = 0.3\ eV$ *and* $E_A = 0.2\ eV$*.*

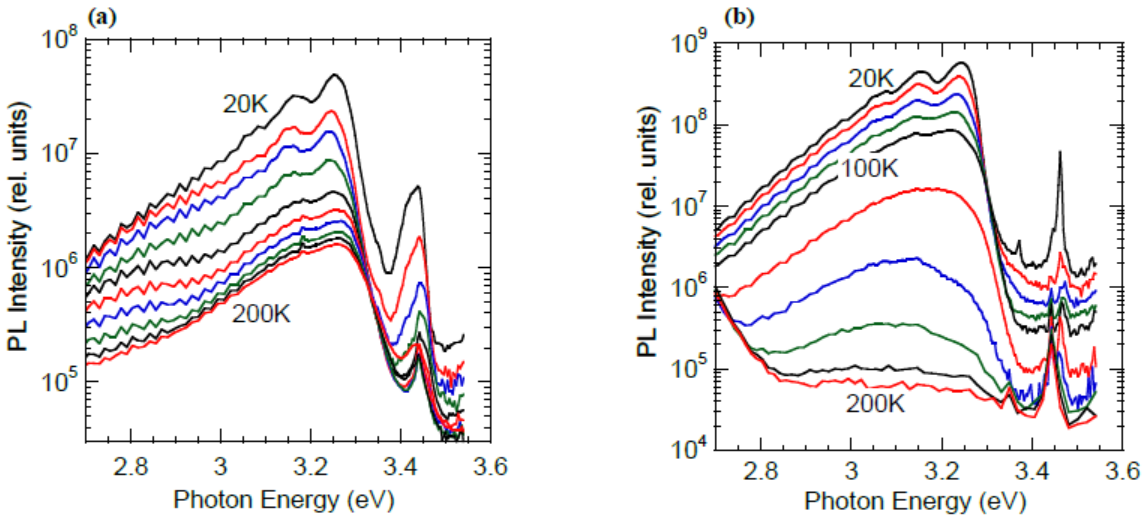

*Figure 2.4-1: Evolution of the PL spectrum in p-type Mg-doped GaN with increasing temperature from 20 to 200 K with step 20 K. (**a**) sample 9600 (group A), (**b**) sample 9591 (group B).* $P_{exc} = 0.3\ W/cm^2$*. The weak oscillations with a period of about* $35\ meV$ *are due to Fabry-Perot effect in the sapphire/GaN/air cavity, revealing the total thickness of GaN layers to be about* $7\ \mu m$*. Figure and caption are both taken from Ref.* 14*.*

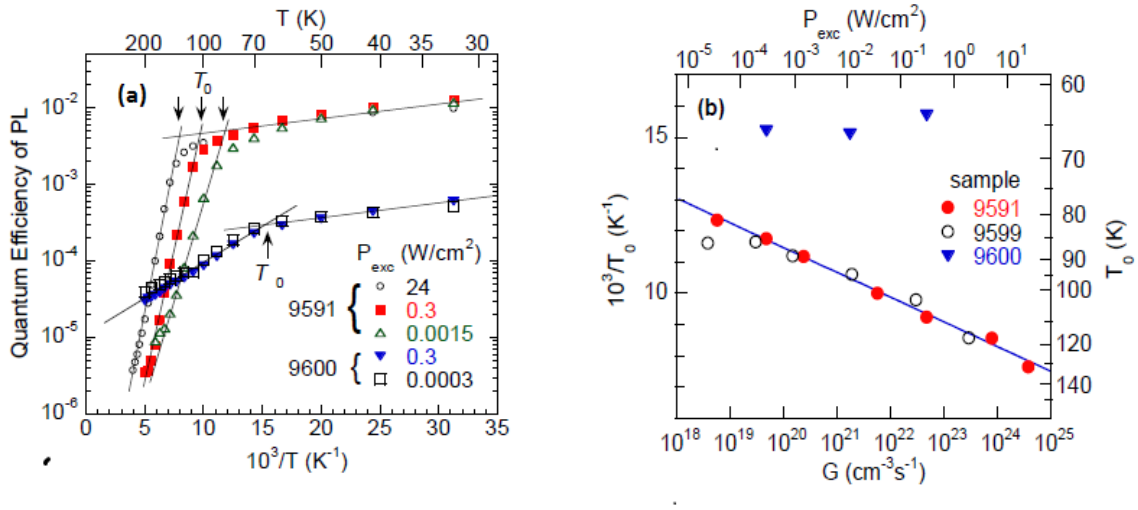

*Fig. 2.4-2: (**a**) Temperature dependence of quantum efficiency of the UVL band in p-type Mg-doped GaN for different $P_{exc}'s$. The lines are extrapolations of the low-temperature and high-temperature parts with an intersection at the characteristic temperature (T_0). For sample 9591 (group B), T_0 shifts with increasing excitation intensity, whereas, for sample 9600 (group A), it does not. (**b**) Dependence of the characteristic temperature T_0 on excitation intensity for the UVL band in three Mg-doped GaN samples. The line is calculated using equation (2.4-1) with $E_A = 250\ meV$ and $B = 3{\times}10^{34} cm^{-3}s^{-1}$. Figure and caption are both taken from Ref.* 14.

3. Experimental Details

3.1 Sample

Free-standing Mg-doped GaN with a thickness of $\sim 0.51\ mm$ was grown by Kyma Technologies on sapphire template. GaN layer self-separates from the sapphire upon cooldown from the HVPE growth temperature. From a set of Mg-doped GaN samples, one sample (AB3589) was chosen for the detailed study included in this thesis. Magnesium concentration in this sample is estimated from secondary-ion mass spectrometry (SIMS) to be $1.5\times10^{18}\ cm^{-3}$. Concentrations of Oxygen (O), Carbon (C), Silicon (Si) and Hydrogen (H) in this sample are $1.7\times10^{16}\ cm^{-3}$, $\sim 1.0\times10^{16}\ cm^{-3}$, $< 4.0\times10^{16}\ cm^{-3}$ and $1.0\times10^{18}\ cm^{-3}$ respectively, from SIMS analysis.

3.2 Experimental set-up

Various optical and electronic elements are required to take PL measurements. We used steady-state PL to study GaN. The set-up includes an excitation source, cryostat, monochromator, detector and other optical accessories such as filters, lenses, etc.

A $325\ nm$ He-Cd laser with power $50\ mW$ and photon energy $3.81\ eV$ was used as the source of excitation intensity. A schematic diagram of the set up that was used in our lab to take the PL measurement is shown in Fig. 3.2-1. Laser light is directed to the sample inside a cryostat after passing through neutral density filters, which are used to

attenuate the laser intensity. Generally, the study of the PL spectrum at various excitation intensities gives many insights into the properties of defects. The PL spectrum at different excitation intensities can be obtained by changing filters on the way of incident laser light. To obtain a very high excitation intensity (e.g., $P_{exc} = 4.2\ W/cm^2$), a converging lens was used to focus the incident light in a comparatively small area on the sample. In fact, excitation intensity up to $200\ W/cm^2$ can be achieved using the focused beam with diameter $0.1 - 0.2\ mm$.

To obtain PL spectra from the sample at various temperatures, an optical cryostat was used where the desired temperature of the sample inside the cryostat was obtained by using a heater and temperature controller. The sample was sandwiched between the copper holder and a flat sapphire window. To ensure better thermal contact between sample and copper plate, an indium film was placed in between. The sapphire window allows us to see interference rings on the sample during the sample installation. Then, the sample can be installed with low and uniform stress by ensuring that interference rings are nearly concentric. A turbomolecular pump was used to extract the air from the cryostat to thermally isolate the sample from the environment. Then the cryostat was cooled down to a temperature of $13.5\ K$ with the help of compressor. Once this temperature was achieved, the desired temperature between $13.5\ K$ and $320\ K$ could be obtained with an electrical heater.

Once the laser light is incident on the sample and absorbed in a thin layer near the surface, PL is emitted in various directions. A small portion of PL was directed towards the monochromator by a series of lenses called a condenser. A monochromator is an optical device which transmits a specific band of radiation and

selects a single wavelength. A schematic picture of a monochromator is shown in the Fig. 3.2-2. It consists of a rotating diffraction grating, slits, and two concave mirrors. PL entering from the entrance slit is reflected onto the grating element by a collimating mirror. The grating element disperses light by diffracting different wavelengths at different angles. The dispersed light is incident on the focusing mirror which reflects the light of different colors to the exit slit. In Fig. 3.2-2, the grating element is positioned in such a way that only a specific color of light (green in this case) can exit the slit and all other colors are blocked. The desired color of light from the monochromator is achieved by rotating the grating.

PL passed through the monochromator is detected by an attached photomultiplier tube (PMT). A PMT is a photoemissive device which is used to detect very weak light signals. PMT consists of electrodes that are contained in a vacuum glass tube. Fig. 3.2-3 shows a schematic of a PMT. Photomultiplier electrodes are basically of three types inside the tube. One is photocathode which produces an electron once the photon hits it as a result of the photoelectric effect. This electron is then directed towards electron multiplier area (or in other words, this electron is attracted by high voltage). The electron multiplier area consists of several anodes called dynodes. Dynodes increase the number of electrons by the process of secondary emission. Each dynode has more positive voltage than the previous one to produce the electron multiplication effect. The dynode chain is designed in such a way that each dynode cascades electrons to successive dynodes and finally to the anode. Once millions of electrons produced due to each photon through this process arrive at the anode, a sharp rise in current is detected. The number of electrons detected by PMT is

proportional to the number of photons that hit the photocathode. Therefore, PL intensity is measured in relative units. These raw data are graphed as intensity vs. wavelength by a computer program called Synergy. Finally, raw data are copied to another program called Kaleidagraph where they are plotted as intensity (in relative units) vs. photon energy for initial graphical interpretations.

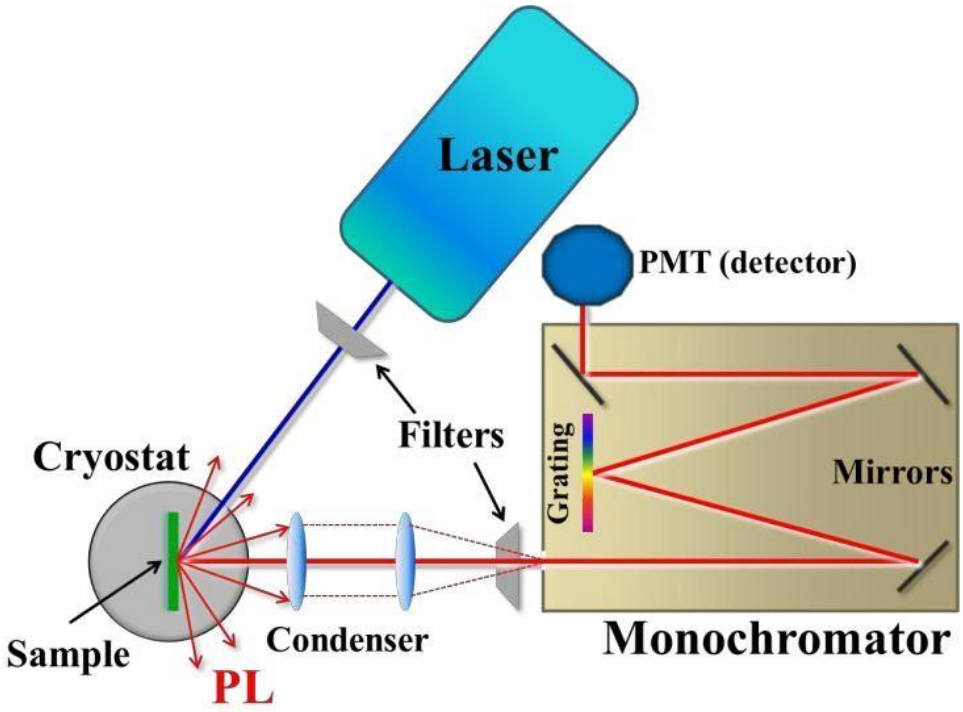

Fig. 3.2-1: Experimental set up for PL measurements. (Courtesy of Joy McNamara)

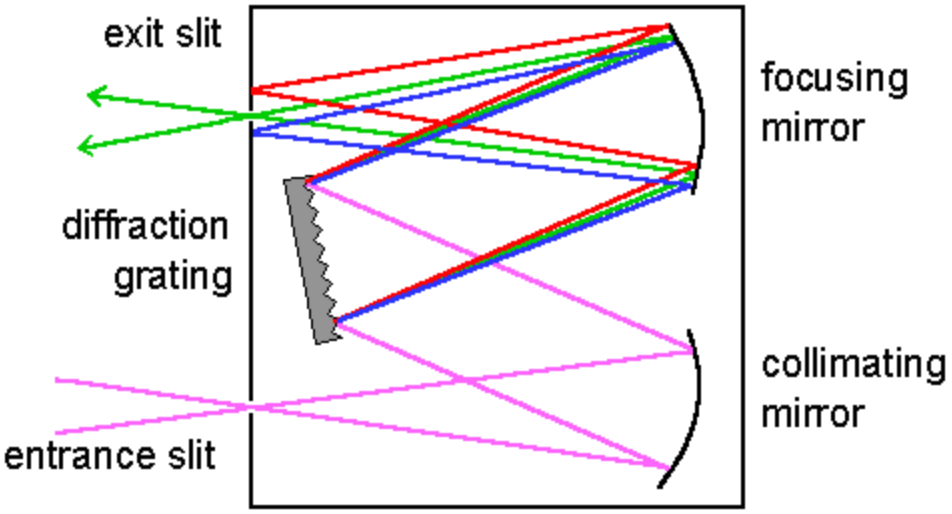

Fig. 3.2-2: Detailed schematics of a monochromator.

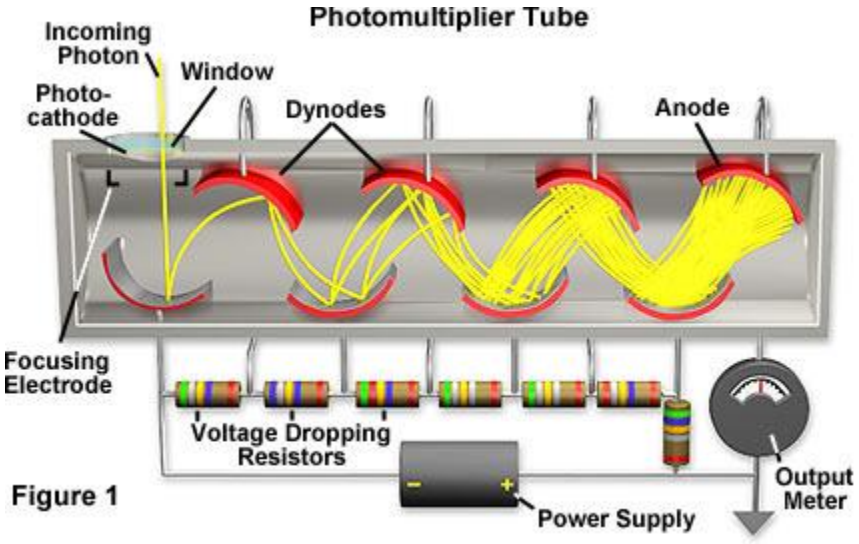

Fig. 3.2-3: Simplified view of a photomultiplier tube.
(https://micro.magnet.fsu.edu/primer/digitalimaging/concepts/photomultipliers.html)

4. Results and Discussion

4.1 PL spectra

From previous experience, we know that illumination of GaN sample at different temperatures and excitation intensities provides the PL spectra of quite distinct nature. Further analysis of the PL spectra gives insights on different aspects, e.g. the nature of the band, energy levels of the donors and acceptors responsible for the band, etc. Following the trend, the sample was illuminated under various temperatures and excitation intensities. Temperature was kept fixed while varying the excitation intensity, whereas excitation intensity was kept fixed while varying the temperature.

Three PL bands, namely exciton band, ultraviolet luminescence (UVL) band and blue luminescence (BL) band can be seen in the Fig. 4.1-1 which shows the PL spectra obtained at various excitation intensities and at $T = 13.5\ K$. Exciton band and UVL band efficiency (i.e., PL intensity divided by the excitation intensity) decreases with decreasing excitation intensity. UVL band also becomes broader with decreasing excitation intensities. A BL band starts appearing with decreasing excitation intensity below $P_{exc} = 0.0002\ W/cm^2$ and becomes more distinct at lower excitation intensities. The BL band shifts to lower energy, while exciton and UVL bands seem to have almost constant positions as excitation density decreases. The detailed study of the PL spectra with excitation intensities is given in Sec. 4.3.

Figs. 4.1-2, (a) to (e), show the PL spectra obtained at different temperatures for fixed excitation intensity. The same Exciton, UVL and BL bands are the major bands of

the spectra in all figures. UVL band intensity decreases with increasing temperature. Exciton band intensity also decreases with increasing temperature until a certain temperature after which it again starts to increase. This temperature at which exciton band intensity again starts to increase is slightly different for different excitation intensities. The BL band can't be seen at low temperature (at relatively high P_{exc}), possibly because it is hidden under the stronger UVL band. As temperature increases, the BL band appears. Its intensity decreases with increasing temperature. The BL band also redshifts with increasing temperature. Below $P_{exc} = 0.0002\ W/cm^2$ (Figs. 4.1-2 (c), (d) and (e)), BL band intensity starts dropping at a much faster rate above some temperature (will be called critical temperature in section 4.4) than the rate below this temperature. The detailed study of PL spectra as a function of temperature will be presented in Sec. 4.4.

Furthermore, a green luminescence (GL2) band appears as a shoulder (at $150\ K$ for $P_{exc} = 0.2\ W/cm^2$) with the apparent maximum at $\approx 2.38\, eV$. At higher temperatures, this shoulder becomes the GL2 band. The intensity of the GL2 band seems almost fixed for some range of temperatures and then gradually decreases with increasing temperature.

As can be seen in the Fig. 4.1-1, the BL band, which is quite distinct from the UVL band at low excitation intensities is almost unseen at higher excitation intensities. Also, the BL band which is quite distinct at high temperatures becomes almost undistinguishable at lower temperatures (see Figs. 4.2-1 (a) and (b)) for relatively higher excitation intensities. This might have happened due to two reasons. The first reason could be that there is no BL band in the spectra of higher excitation intensities (Fig. 4.1-

1) and lower temperatures (Figs. 4.2-1 (a) and (b)). The second (and most probable) reason is that the BL band is similar to the UVL band in shape and position, but has a relatively small contribution in the spectrum as compared to the UVL band, so that it gets weakened in the spectrum and can't be seen. The second reason is the most probable one because if we look at the nature of the BL intensity, it is clearly seen that the BL contribution increases with increasing excitation intensity (Fig. 4.1-1) and its intensity decreases with decreasing temperatures (Fig. 4.1-2) and it is quite unreasonable to assume that it suddenly disappears at low temperatures or high excitation intensities. To see the BL contribution at low temperature and high excitation intensity, we used deconvolution method that allows us to separate the BL band and the UVL band. The detailed procedure on the deconvolution is discussed in Sec. 4.2.

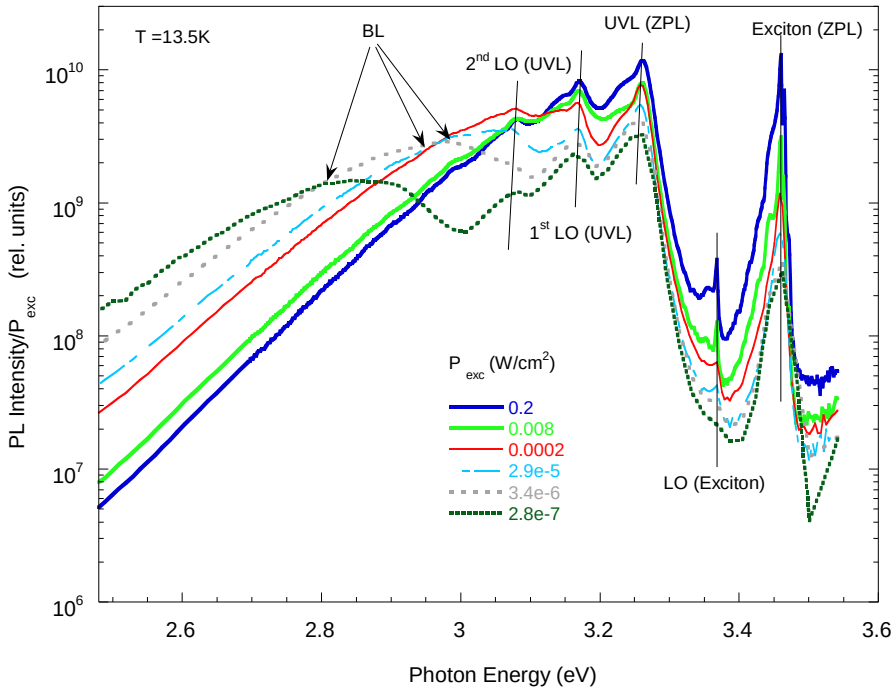

Fig. 4.1-1: PL spectra at different excitation intensities. PL intensities are divided by excitation intensities under the same conditions so that intensities of each spectrum are relative to each other. Exciton peak is at 3.467 eV followed by LO phonon replica at 3.374 eV. The UVL peak has ZPL at 3.267 eV followed by two phonon replicas at 3.177 eV and 3.085 eV. The BL band appears at excitation intensities below $0.0002\ W/cm^2$. *The BL band blueshifts with increasing excitation intensity.*

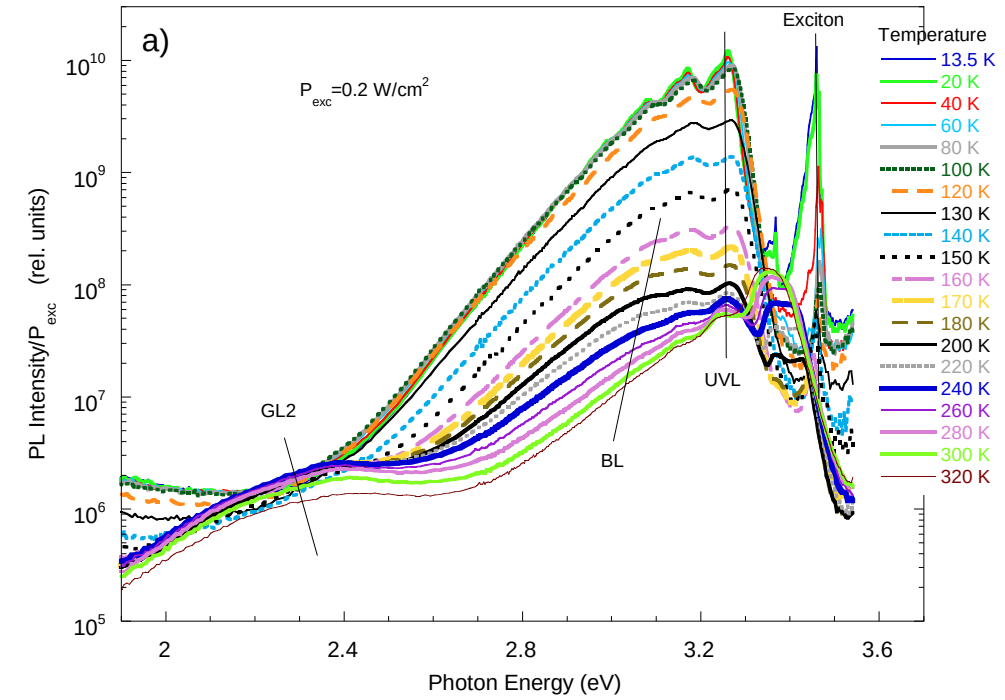
a)
P_{exc}=0.2 W/cm^2
Exciton
UVL
BL
GL2
Temperature
13.5 K
20 K
40 K
60 K
80 K
100 K
120 K
130 K
140 K
150 K
160 K
170 K
180 K
200 K
220 K
240 K
260 K
280 K
300 K
320 K
PL Intensity/P_{exc} (rel. units)
Photon Energy (eV)

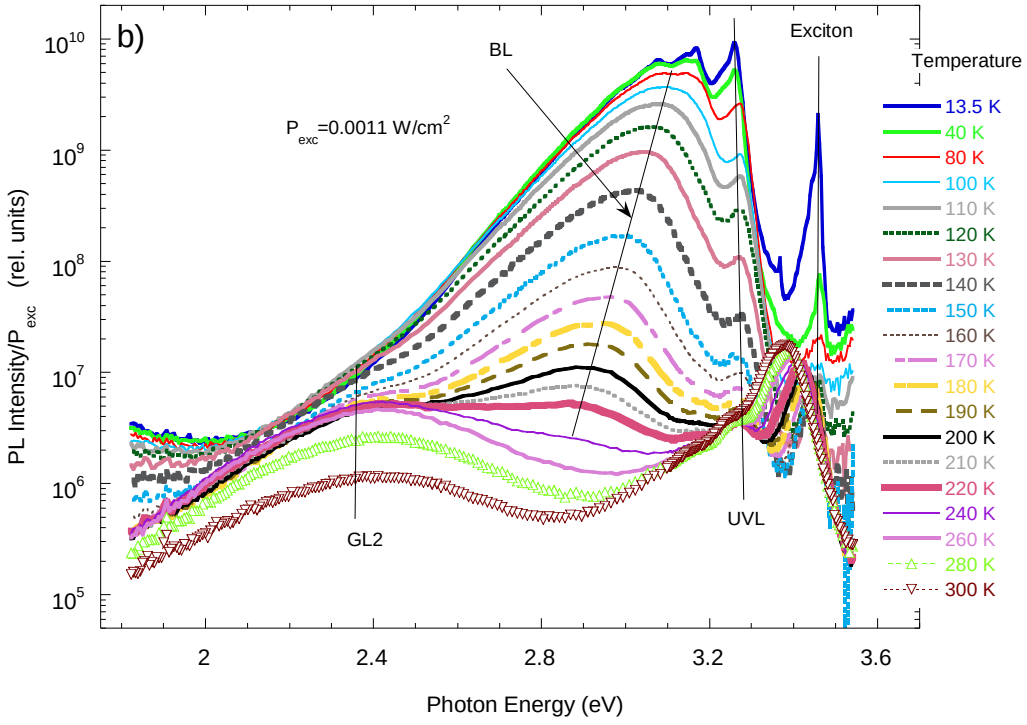
b)
P_{exc}=0.0011 W/cm^2
BL
Exciton
UVL
GL2
Temperature
13.5 K
40 K
80 K
100 K
110 K
120 K
130 K
140 K
150 K
160 K
170 K
180 K
190 K
200 K
210 K
220 K
240 K
260 K
280 K
300 K
PL Intensity/P_{exc} (rel. units)
Photon Energy (eV)

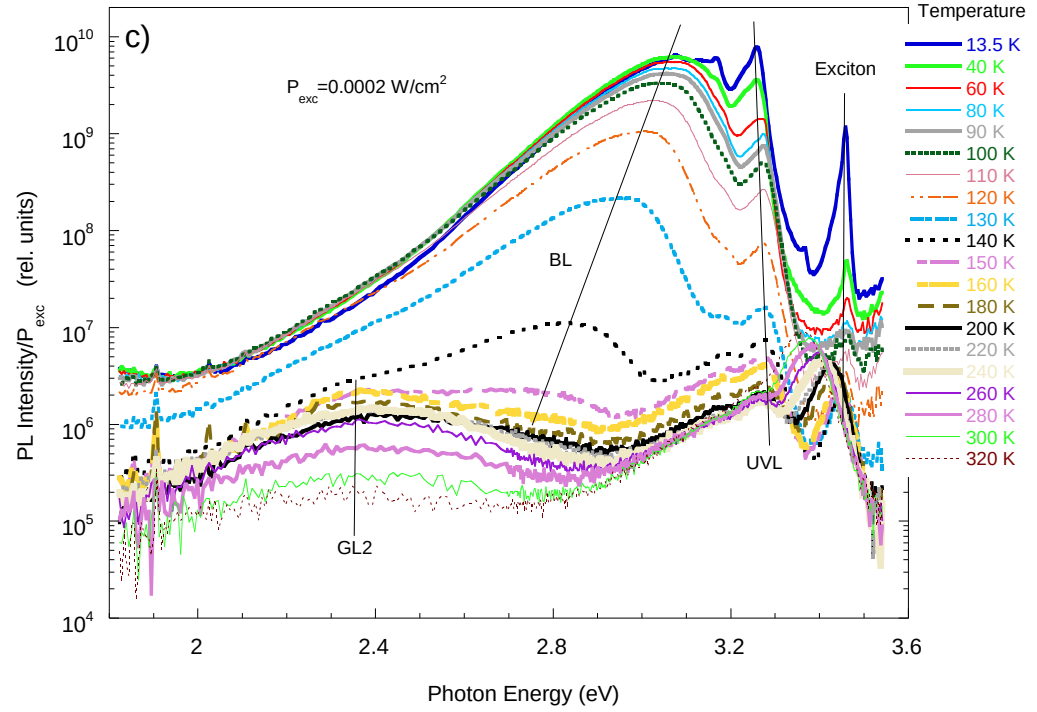
c)
P_exc=0.0002 W/cm^2
Exciton
BL
UVL
GL2
PL Intensity/P_exc (rel. units)
Photon Energy (eV)
Temperature
13.5 K
40 K
60 K
80 K
90 K
100 K
110 K
120 K
130 K
140 K
150 K
160 K
180 K
200 K
220 K
240 K
260 K
280 K
300 K
320 K

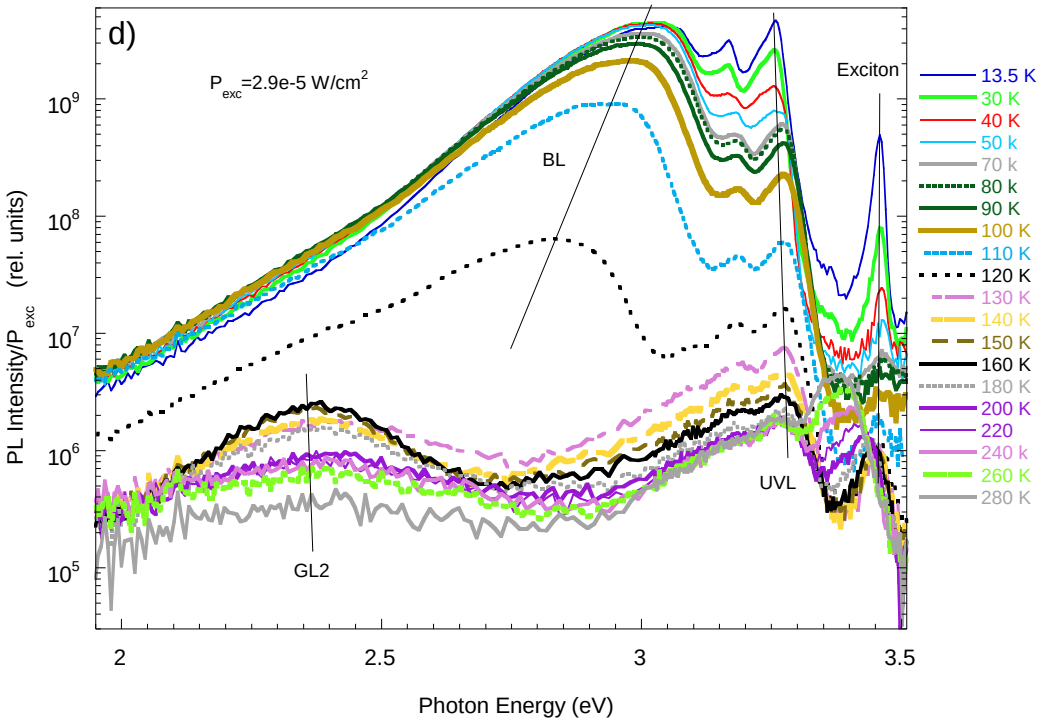
d)
P_exc=2.9e-5 W/cm^2
Exciton
BL
UVL
GL2
PL Intensity/P_exc (rel. units)
Photon Energy (eV)
13.5 K
30 K
40 K
50 k
70 k
80 k
90 K
100 K
110 K
120 K
130 K
140 K
150 K
160 K
180 K
200 K
220
240 k
260 K
280 K

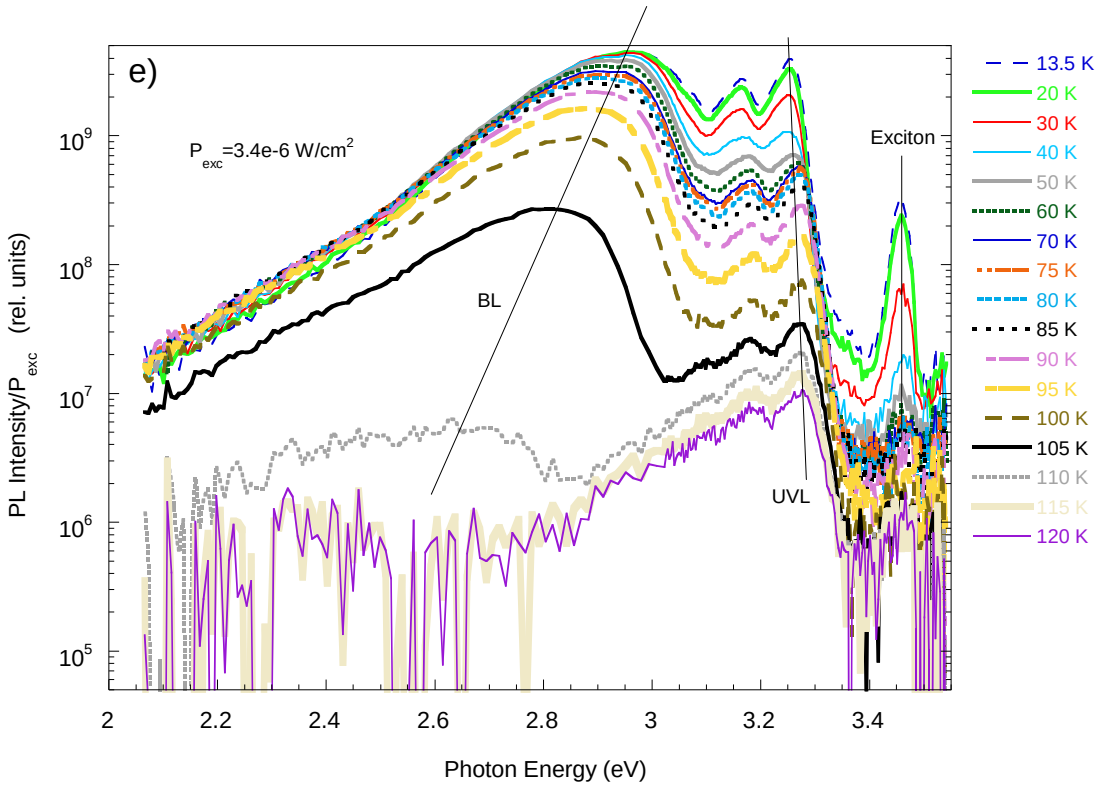

Fig. 4.1-2: PL spectra at various temperatures but fixed excitation intensity. In all figures, BL band starts appearing distinctly with the increase in temperature except in (a) where BL band is seen as the shoulder on the tail of UVL band at best. The BL band can be seen distinctly even at T=13.5 K for low excitation intensities e.g. in figure (d) and (e). BL band is unseen (or not clearly distinct from UVL) at low temperatures possibly because it hides under the stronger UVL peak. Exciton and UVL band intensities decrease with increasing temperature. BL intensity also decreases with increasing temperature. However, in figs (c), (d) and (e) BL intensity drop is quite abrupt after temperature reaches certain value. These characteristic temperatures (at which abrupt drop begins) are different for different excitation intensities. The GL2 band can be found at all figures except (e) at about 2.38 eV.

4.2 Deconvolution of PL spectra

Deconvolution basically means resolving a PL spectrum representing a superposition of several bands (e.g., Red, Blue, UVL, Exciton, etc) into constituent bands so that it will be easier to study the properties of individual bands.

Below, we explain how PL spectra were deconvoluted to obtain the contribution of the BL band. For the deconvolution purpose, we used a PL spectrum (called model UVL) which has a very large contribution of the UVL band compared to the BL band. Since exciton band appears distinctly separate from the UVL band, we don't need to worry about the contribution of this band and no separate deconvolution is needed to find the model UVL containing only UVL band. We call this spectrum a model UVL and we will subtract this spectrum from PL spectrum that needs deconvolution.

We obtained model UVL by exciting the sample AB3589 (the same sample that is studied in detail in this work) at various temperatures with the focused beam ($P_{exc} = 4.2\ W/cm^2$). We obtained focused beam using a focusing lens (focal length $\approx\ 14 - 15\ cm$). Initially, a laser beam from He-Cd laser was passed through a neutral density filter (attenuation$= 0.042$) before the lens. Lens focuses the laser beam of diameter about $4\ mm$ into a diameter of $0.1 - 0.2\ mm$ on the sample. As a result, the beam that is incident on the sample has the power density $P_{exc} = 4.2\ W/cm^2$. At such high excitation density, the BL band saturates due to relatively long life-time and the PL spectrum represents almost only the UVL band.

To illustrate the detailed procedure on how we conducted deconvolution to resolve the BL band, three representative PL spectra are shown as examples. Figs. 4.2-1 (a) and (b) show the PL spectra at same excitation intensity ($P_{exc} = 0.2\ W/cm^2$) but

at different temperatures. Fig. 4.2-1 (c) shows PL spectrum at $P_{exc} = 2.9\times 10^{-5}\ W/cm^2$and at $T = 110\ K$. Model UVL in all three figures was obtained at the same temperatures as the PL spectrum. Though model UVL was acquired at different excitation intensity than that of PL spectra, we know from previous experience that shape of pure UVL doesn't change much with excitation intensity for a specific temperature. Therefore, model UVL was matched with the UVL band maximum in PL spectra by adjusting its intensity. Additionally, a small shift of the model UVL band along the horizontal axis (by not more than $6-7\ meV$) was made to better match position of the UVL band maximum. This shift is justified because it is known that the UVL band may shift by several meV to higher photon energies with increasing P_{exc} due to different reasons. [16]

In the next step, model UVL shape was subtracted from PL spectra, and the subtracted data were plotted to get the new spectrum which has no contribution of UVL or, in other words, the contribution of BL band was determined in the spectrum. Deconvoluted PL spectra are displayed in Figs. 4.2-2 (a), (b) and (c). We can see in the Figs. 4.2-2 (a) and (b) the presence of several kinks in the intensity at the right side of deconvoluted PL. Several kinks in the deconvoluted spectrum are caused by imperfect match (the UVL shape slightly changes with variation of excitation intensity) between model UVL and real UVL band in PL spectra (Fig. 4.2-3).

It is still difficult to find precisely the peak position, maximum intensity, and shape of the BL band after the deconvolution, because the deconvoluted spectrum contains several kinks. To eliminate or reduce this deficiency, the deconvoluted PL spectra were fitted with the following expression,[18]

$$I = I_{max}\exp[-2S_e\left(\sqrt{\frac{E_0+\frac{1}{2}\hbar\Omega-\hbar\omega}{E_0+\frac{1}{2}\hbar\Omega-\hbar\omega_{max}}}-1\right)^2]. \quad (4.2\text{-}1)$$

Here, I_{max} is the maximum intensity of the band, E_0 is zero phonon line energy of BL band, $\hbar\Omega$ is the energy of dominant phonon mode and $\hbar\omega_{max}$ is the energy of maximum of BL band. S_e is called Huang-Rhys factor. S_e and $E_0+\frac{1}{2}\hbar\Omega-\hbar\omega_{max}$ determine the shape of the band. When the values of $E_0+\frac{1}{2}\hbar\Omega$ and $\hbar\omega_{max}$ are changed simultaneously by Δ, the band shifts by the same Δ without changing the shape. Figs. 4.2-4 (a), (b) and (c) show the deconvoluted PL spectrum with the fit using Eq. (4.2-1).

The UVL band is attributed to the transition between shallow donor (O_N or Si_{Ga}) and shallow acceptor (Mg_{Ga}) at low temperature and the transition between the conduction band and Mg_{Ga} acceptor (eA transition) at high temperature.[16] In p-type GaN, Fermi level is close to the Mg_{Ga} acceptor. Therefore, shallow donors are almost empty of electrons. As a result, in P-type GaN, UVL contribution is mostly due to eA transitions even at low temperature. The BL band is attributed in literature to the transition between unknown deep donor and Mg_{Ga} acceptor.[2,4,19] Life-time of transition between deep donor and Mg_{Ga} acceptor is roughly three orders of magnitude greater than the life time of eA transition according to time-resolved PL measurements. So, with increasing excitation intensity, BL transition saturates much faster than the eA transition. Hence, UVL band is dominant in the spectrum obtained at high excitation intensity. This is the reason why we need to find the shape of the model UVL band. Though deconvoluted PL spectra obtained at low excitation intensity as in Fig. 4.2-2 (c) match with original PL spectra because of small contribution of UVL band and almost all features of BL band, e.g. intensity maxima, energy of band maxima etc., can be

obtained with original PL spectra, it is still useful to deconvolute the PL spectra for self-consistency.

BL bands at various excitation intensities but the same temperature are normalized and shifted to the same position to compare the shapes in Fig. 4.2-5. It can be seen from the figure that the BL band becomes wider with decreasing excitation intensity, which is reasonable for any model of the BL band. For example, the broadening may happen with decreasing excitation intensities due to significant potential fluctuations which facilitate the wide range of transitions (i.e. vertical and diagonal). In another model, narrowing of the BL band with increasing excitation intensity may happen because of the saturation of more distant DAP with increasing excitation intensities. As excitation intensity decreases, BL is produced by transitions between various DAPs that range from close to distant. This results in broadening of the band. The moderate broadening of the BL band proves that the deconvolution method we use to find the contribution of BL band in the PL spectra is reliable.

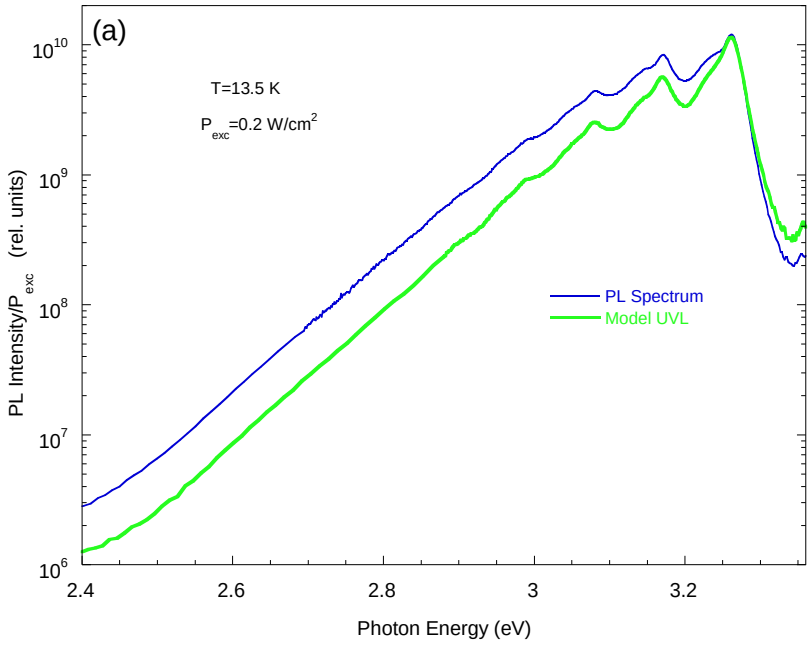

Fig. 4.2-1 (a): PL spectrum (at $P_{exc} = 0.2\ W/cm^2$) and model UVL at $T = 13.5\ K$. Model UVL is reduced in intensity and shifted towards left to match the UVL band of PL spectrum.

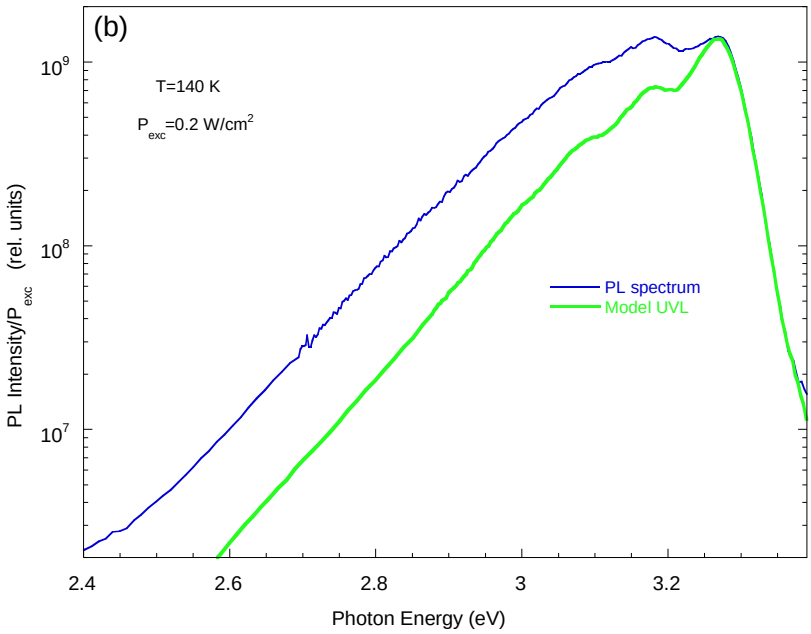

Fig. 4.2-1 (b): PL spectrum (at $P_{exc} = 0.2\ W/cm^2$) and model UVL at $T = 140\ K$. Model UVL is reduced in intensity and shifted towards left to match the UVL band of PL spectrum. PL spectrum at 140 K is broader than 13.5 K and shows less contribution of UVL band. i.e. BL band is becoming more prominent with temperature.

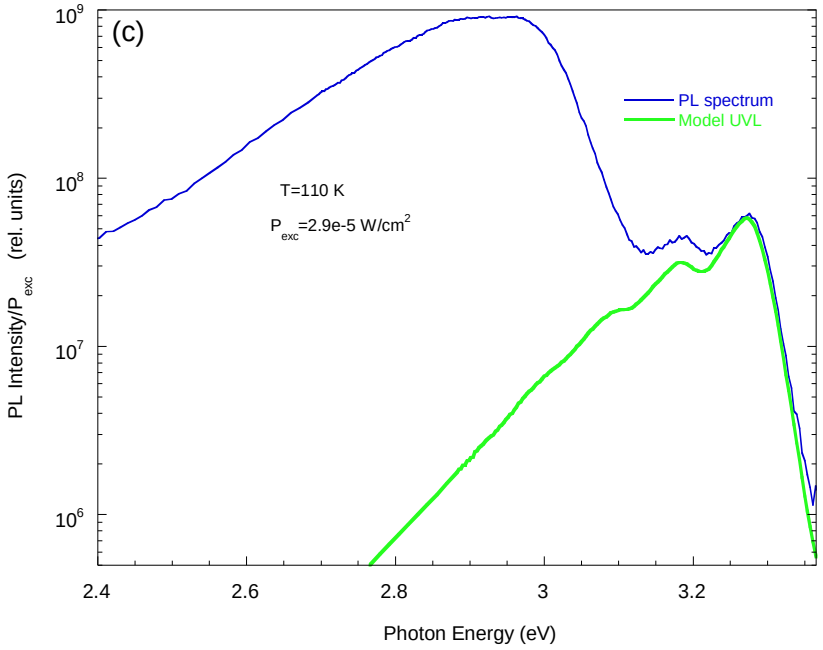

Fig. 4.2-1 (c): PL spectrum (at $P_{exc} = 2.9\times10^{-5}\ W/cm^2$) and model UVL at $T = 110\ K$. Model UVL is reduced in intensity and shifted towards left to match the UVL band of PL spectrum. A noticeable feature in the figure is that with small excitation intensity, BL band clearly separates from the UVL band.

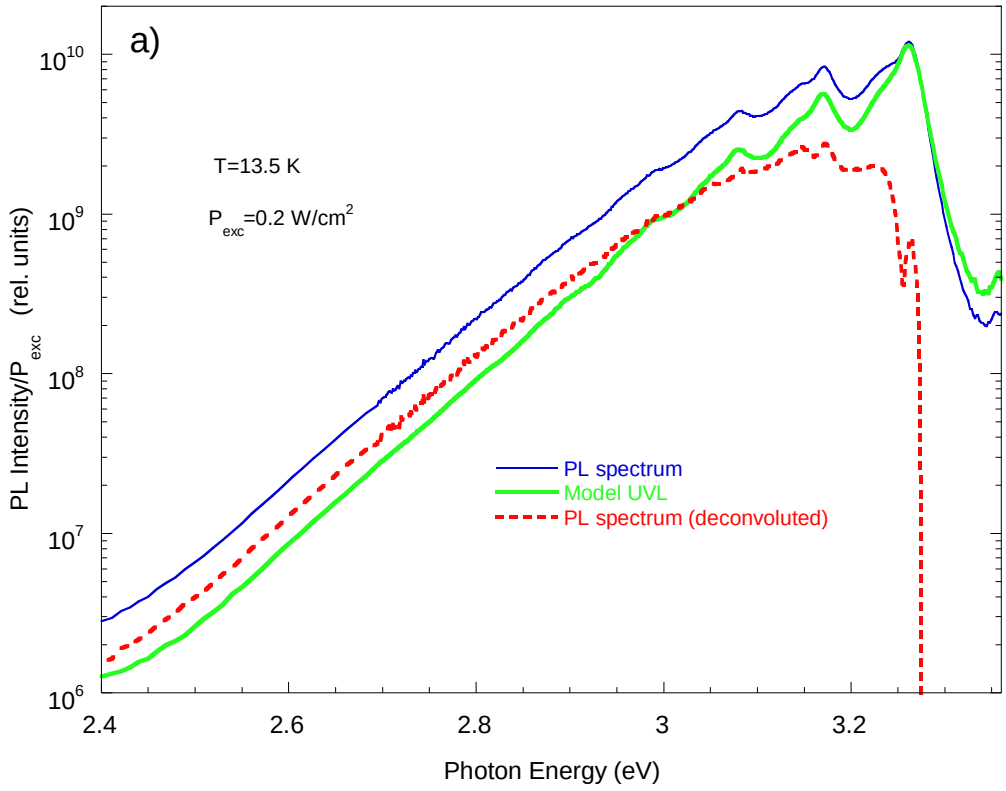

Fig. 4.2-2 (a): Deconvoluted PL spectrum at $T = 13.5\ K$ and $P_{exc} = 0.2\ W/cm^2$. Several kinks in the deconvoluted spectrum arise because of the imperfect match between model UVL and UVL band of PL spectra.

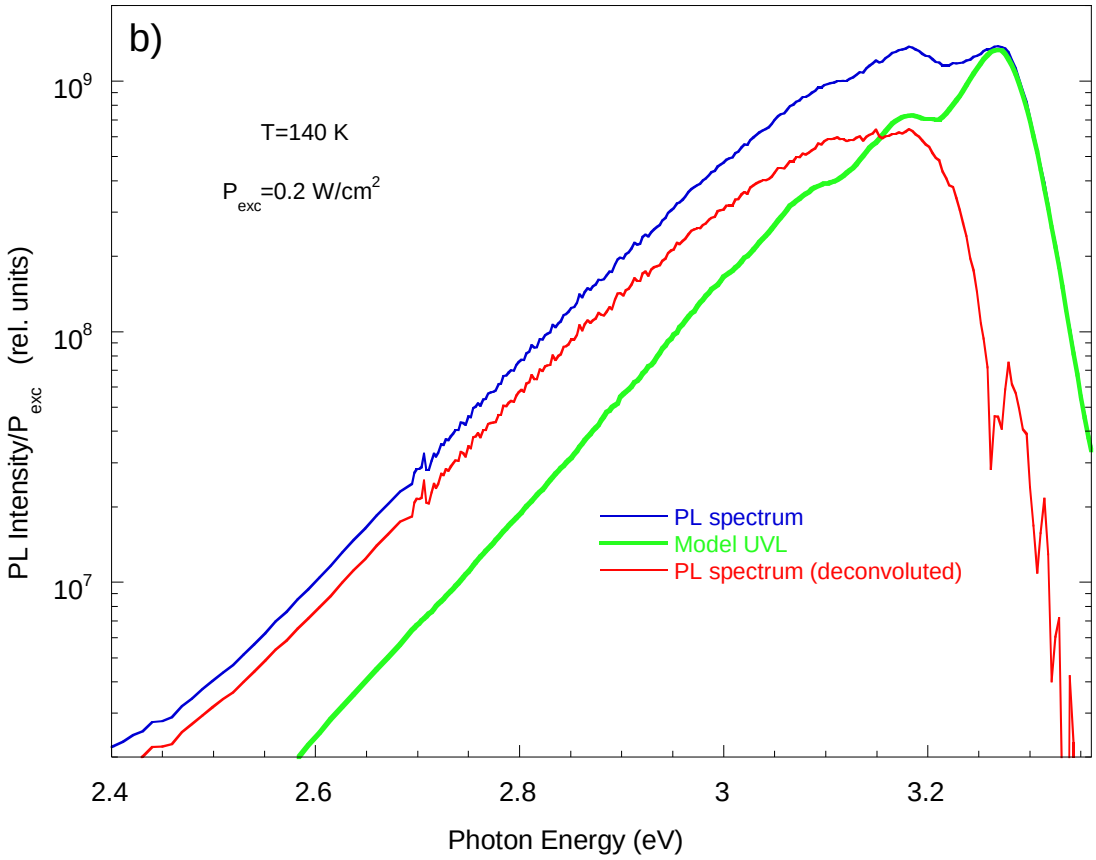

Fig. 4.2-2 (b): Deconvoluted PL spectrum at $T = 140\ K$ and $P_{exc} = 0.2\ W/cm^2$. Several kinks in the deconvoluted spectrum arise because of the imperfect match between model UVL and UVL band of PL spectra.

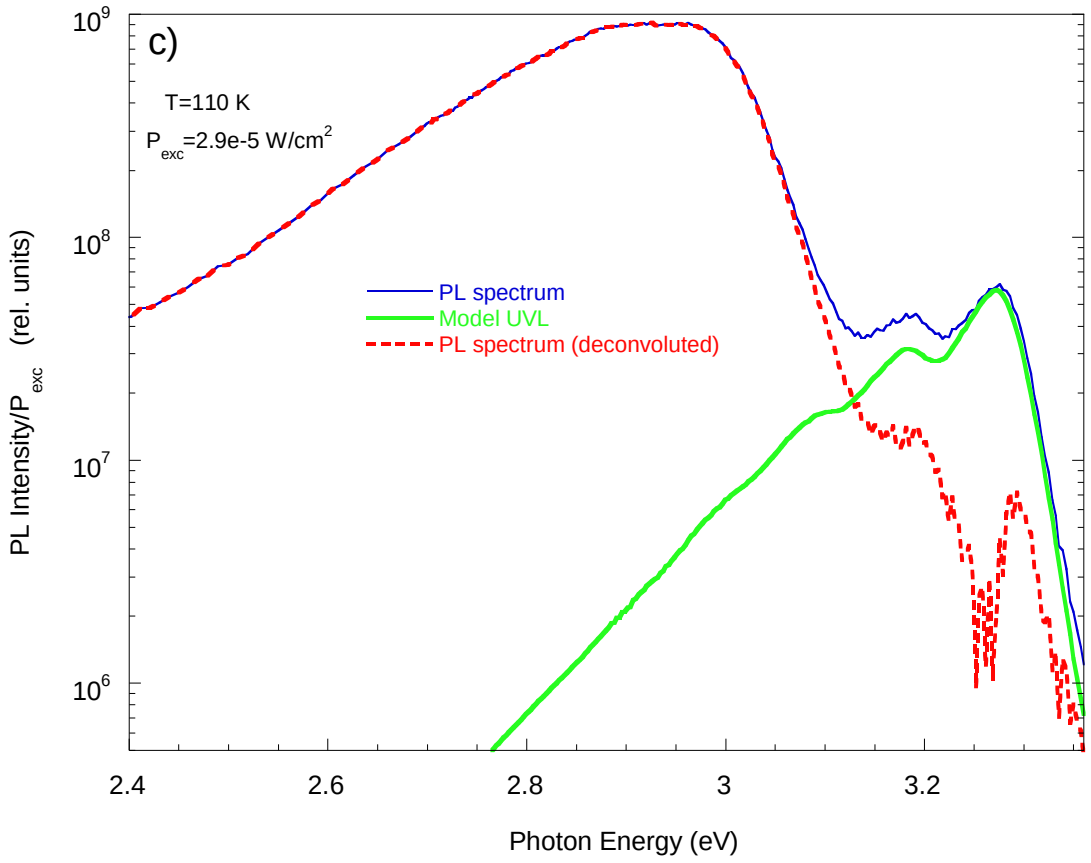

Fig. 4.2-2 (c): Deconvoluted PL spectrum at $T = 110\,K$ and $P_{exc} = 2.9\times10^{-5}\ W/cm^2$. The BL band of PL spectrum and the BL band of deconvoluted PL spectrum match exactly and kinks are also not present in the deconvoluted spectrum (despite the lack of perfect match between model UVL and UVL band of PL spectra) because of the negligible contribution of the UVL band compared to the BL band.

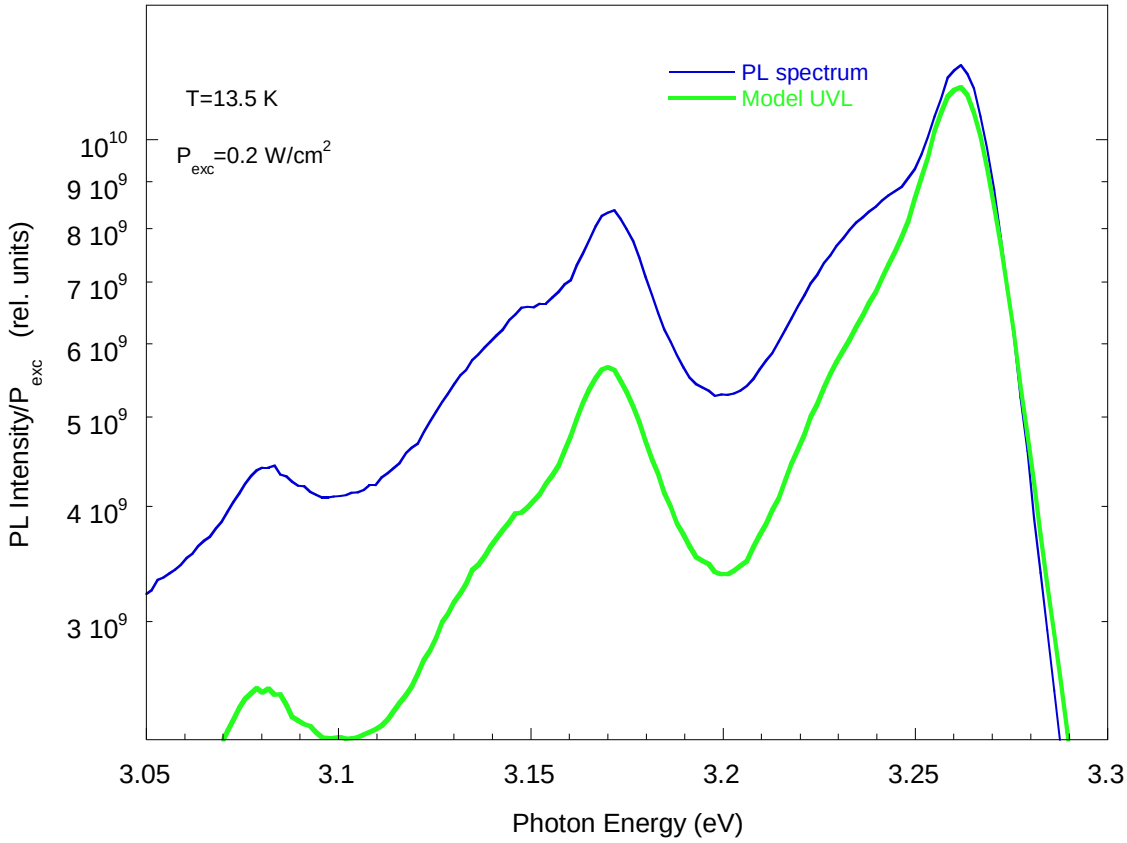

Fig. 4.2-3: Magnified view of the main peak area of model UVL and UVL band of PL spectra of Fig 4.2-1 (a). The imperfect match between these two bands produces kinks while subtracting model UVL from PL spectrum.

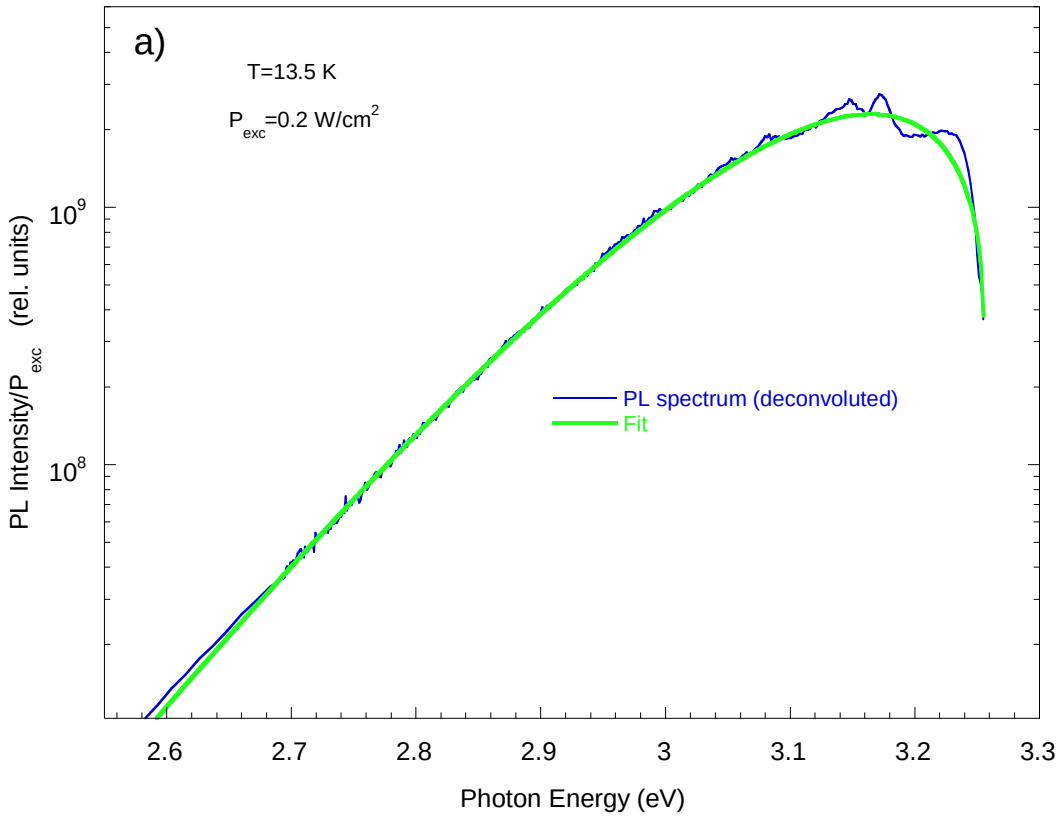

Fig. 4.2-4 (a): Deconvoluted BL band corresponding to Fig. 4.2-2 (a). The fit was obtained using Eq. (4.2-1) with parameters, $I_{max} = 2.3\times10^{9}$, $S_e = 0.92$, $E_0 + \frac{1}{2}\hbar\Omega = 3.255\ eV$ *and* $\hbar\omega_{max} = 3.165\ eV$.

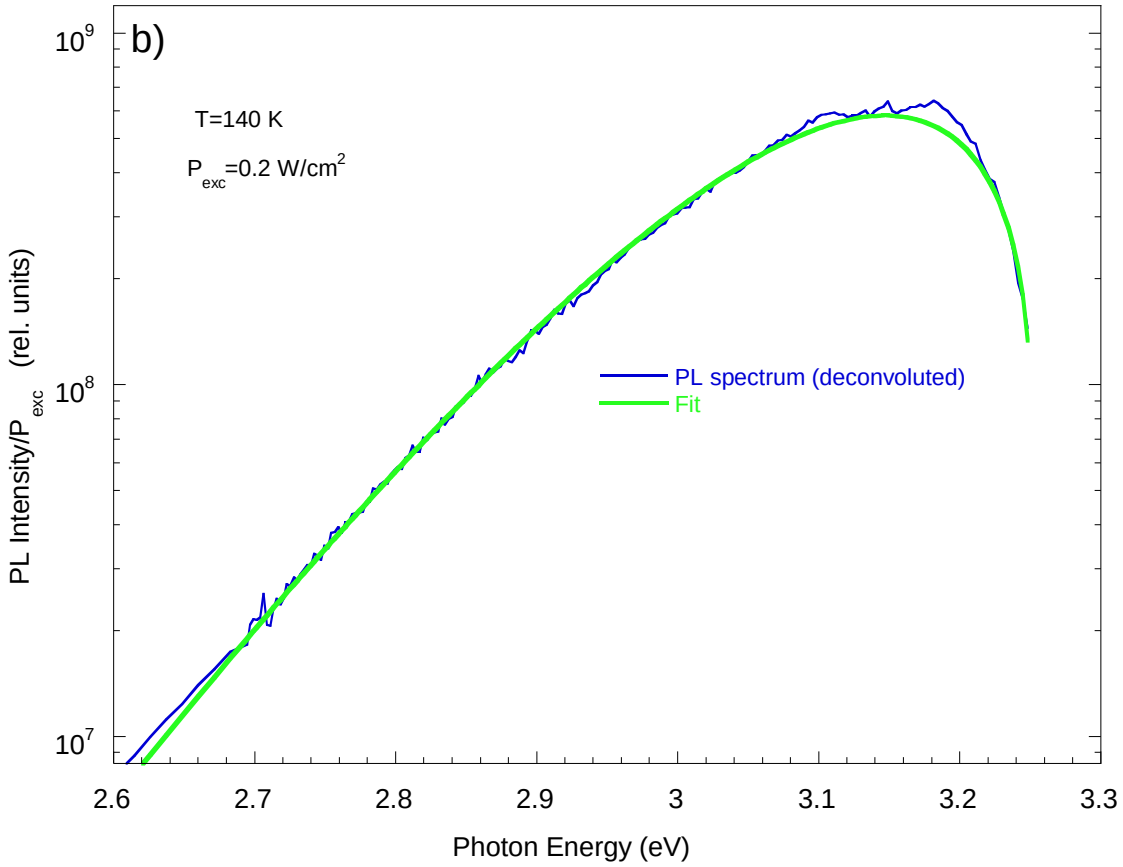

Fig. 4.2-4 (b): Deconvoluted BL band from Fig. 4.2-2 (b). The fit was obtained using Eq. (4.2-1) with parameters, $I_{max} = 5.82\times10^{8}$, $S_e = 0.98$, $E_0 + \frac{1}{2}\hbar\Omega = 3.25\ eV$ *and* $\hbar\omega_{max} = 3.147\ eV$.

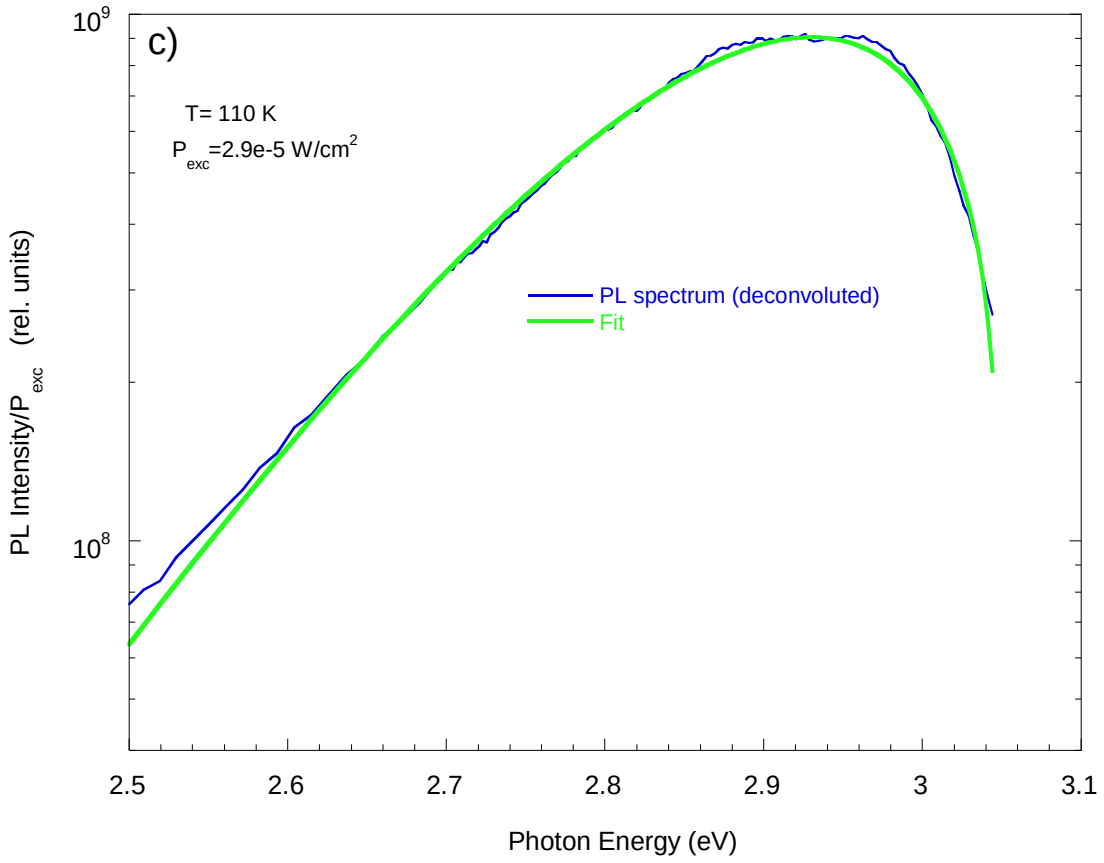

Fig. 4.2-4 (c): Deconvoluted BL band from Fig. 4.2-4 (c). The fit was obtained using Eq. (4.2-1) with parameters, $I_{max} = 9.05\times10^{8}$, $S_e = 0.97$, $E_0 + \frac{1}{2}\hbar\Omega = 3.046\ eV$ *and* $\hbar\omega_{max} = 2.93\ eV$.

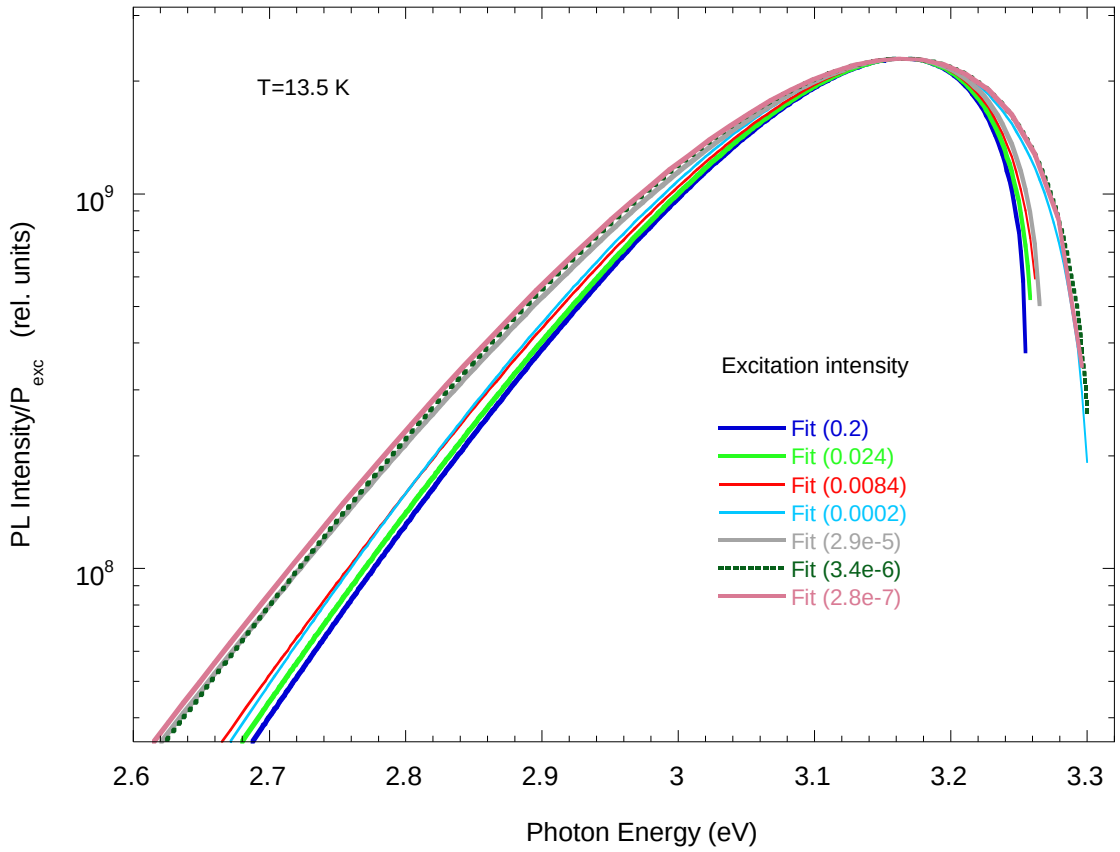

Fig. 4.2-5: Fits to the deconvoluted blue bands using Eq. (4.2-1) at various excitation intensities and $T = 13.5\ K$. Intensities of all spectra are normalized to the spectrum of $P_{exc} = 0.2\ W/cm^2$. Also, energy maxima of all the spectra are shifted to the maximum of $P_{exc} = 0.2\ W/cm^2$ for comparison of shapes.

4.3 Dependence on Excitation intensity:

In our experiments, we studied Mg-doped GaN by illuminating it with He-Cd laser ($325\ nm$). Figure 4.1-1 shows the PL spectra obtained with various excitation intensities but at fixed temperature ($13.5\ K$). All the PL intensities are divided by excitation intensity under the same condition so that intensity of each spectrum is relative to each other. At high excitation intensities ($P_{exc} = 0.2$ and 0.008 W/cm^2) we see the exciton band with the highest peak at $3.467\ eV$ and the UVL band which ranges from $2.5\ eV$ to $3.3\ eV$, with the highest peak at $3.267\ eV$ followed by two LO phonon replicas at $3.177\ eV$ and $3.085\ eV$. With decreasing excitation intensity, contributions of the UVL and exciton bands in the spectra decrease whereas BL band appears at relatively low excitation intensities and its contribution becomes prominent at $P_{exc} = 2.8\times10^{-7}$ W/cm^2. The exciton band having the main peak at $3.467\ eV$ is followed by an LO phonon replica at $3.374\ eV$. At high excitation intensities, another excitonic peak at $3.471\ eV$ can also be seen. This peak disappears as excitation intensity decreases. We believe that these two peaks at $3.467\ eV$ and $3.471\ eV$ are due to the annihilation of acceptor bound exciton (ABE) and donor bound exciton (DBE) respectively. UVL band consisting of the main peak at $3.267\ eV$ followed by phonon replicas was found to broaden with decreasing excitation intensity.

Fig 4.3-1 shows peak positions of different bands as a function of excitation intensity. The UVL and exciton band positions remain almost fixed (within the accuracy of $3\ meV$) with excitation intensity. However, the variation of peak position with the

excitation intensity, as seen in Fig. 4.3-1, is enormous for the BL band. The position of the BL band shifts by almost $0.4\ eV$ and the shift saturates for $P_{exc} > 0.008\ W/cm^2$.

BL band is attributed in literature to the DAP-type transitions from a deep donor to the shallow Mg_{Ga} acceptor.[2,4,19] The UVL band is attributed to transitions from a shallow donor (at room temperature) or the conduction band (at room temperature) to the shallow Mg_{Ga} acceptor.[16] Ionization energies of Mg_{Ga} acceptor and deep donor are $0.15 - 0.2\ eV$ and $0.3 - 0.7\ eV$ respectively.[16,] In this section, we will mainly analyze the variation of the BL band position with excitation intensity by considering the two models which are discussed below.

a) Potential fluctuation model:

Potential fluctuations are expected in high-resistivity or p-type GaN. Broadening and redshift of the PL band with decreasing excitation intensity can be attributed to potential fluctuations if they are present in the sample. Since we have seen both broadening and redshift of the BL band in the PL spectra (Figs. 4.1-1 and 4.3-1), it is reasonable to assume that potential fluctuations play a significant role in PL from our sample.

According to Potential fluctuations model, positions of the zero-phonon line ($\hbar\omega$) of a PL band is given by equation (2.2-5) as [8,9]

$$\hbar\omega = E_g - (E_D + E_A) - 2\gamma, \qquad (2.2\text{-}5)$$

where E_g is the band gap energy, E_D and E_A are ionization energies of donor and acceptor participating in DAP transition, and γ is the amplitude of long-range potential fluctuations. With increase in excitation intensity, more photogenerated electrons and

holes are available in the conduction and valence bands, respectively. These photogenerated charge carriers screen the potential fluctuations. That is, with increasing excitation intensity, fluctuation amplitude (γ) decreases and emission energy increases since there will be more vertical transitions as the diagonal transitions gradually convert into vertical transitions due to the flattening of the potentials (Fig.2.2-1).

In Fig. 4.3-1, we can see that peak position of the BL band shifts to higher energies with increase in excitation intensity. Fluctuations become less strong (i.e. γ decreases) due to screening effect with excitation intensity.[4,16] It can be seen from Fig. 4.3-1 that after $P_{exc} \approx 0.01\ W/cm^2$ that BL peak position saturates at $3.16\ eV$.

Since equation (2.2-5) includes $\hbar\omega$ as the ZPL, not the band maximum, we need to make the corresponding correction. From the fit of the spectra from Fig. 4.1-1 (fit not shown in the figure) with equation (4.2-1), the BL band with a maximum at $3.16\ eV$ has the ZPL at $3.29\ eV$. Therefore, from equation (2.2-5), we can write for highest excitation intensity (assuming $\gamma = 0$)

$$\hbar\omega = E_g - (E_D + E_A) \geq 3.29\ eV.$$

On solving above relation, we get $E_D \leq (0.013 - 0.063)\ eV)$ [for $E_A = (0.15 - 0.2\ eV)$] [16] with $E_g = 3.503\ eV$. The band gap energy ($E_g = 3.503\ eV$ for $T = 13.5\ K$) was calculated from the relation [20]

$$E_g = [3.503 + \frac{5.08\times10^{-4}T^2}{T-996}]. \qquad (4.3\text{-}1)$$

The ionization energy of the donor found by above calculation is much lower than the commonly-considered value of E_D $(0.3 - 0.7\,eV)$ for the deep donor.[16] Some authors have also claimed that broad BL band in Mg-doped sample comes from the transition between the conduction band and a deep acceptor level.[6] With the result that we just found [i.e., $E_D \leq (0.013 - 0.063\,eV)$], this idea demands a consideration. However, this possibility can be rejected in our case because it cannot explain the higher emission energy of BL band at high excitation intensity. The ZPL of the BL band at high excitation intensity (mentioned earlier) is $3.29\,eV$. For the emission energy of 3.29 eV, the acceptor ionization energy should be less than $0.21\,eV$ which is almost equal to the ionization energy of shallow Mg_{Ga} acceptor. Hence, the idea that BL band is due to transitions from the conduction band to a deep acceptor level cannot be entertained in our case.

b) Donor Acceptor Pair model:

The shift of the BL band can also be explained as saturation of PL from distant DAP due to their longer lifetime. For distant DAP, the dependence of the zero-phonon line ($\hbar\omega$) on the pair separation (R) is given by equation (2.3-1) as [11]

$$\hbar\omega = E_g - (E_d + E_A) + \frac{q^2}{4\pi\epsilon_0\epsilon R}\,. \qquad (2.3\text{-}1)$$

All the parameters in the above equation have been described in Section 2.3.

For DAP model, Zacks and Halperin[12] developed a theoretical relation between the dependence of the ZPL and the excitation energy assuming that one of the defects has a larger Bohr radius than another. This relation is given by equation (2.3-2) as

$$P_{exc} = D\frac{(\hbar\omega-\hbar\omega_\infty)^3}{\hbar\omega_B+\hbar\omega_\infty-2\hbar\omega}e^{\left(-2\frac{(\hbar\omega_B-\hbar\omega_\infty)}{\hbar\omega-\hbar\omega_\infty}\right)}. \quad (2.3\text{-}2)$$

All the parameters in the above equation have been described in section 2.3. According to this equation, $\hbar\omega = \frac{1}{2}(\hbar\omega_B + \hbar\omega_\infty)$ when $P_{exc} \to \infty$ (i.e. at very high excitation intensity) and $\hbar\omega = \hbar\omega_\infty$ as $P_{exc} \to 0$ (i.e. at very low excitation intensity). The total shift of the band between low and high excitation intensity is $\frac{1}{2}(\hbar\omega_B - \hbar\omega_\infty)(= \frac{1}{2}E_B)$. Hence, shift of the band should be in the limit,

$$0 \le shift \le \frac{1}{2}E_B. \quad (4.3\text{-}2)$$

From Fig. 4.3-1, we see that the shift of the BL band between low excitation intensity ($P_{exc} = 2.8\times10^{-8}\ W/cm^2$) and high excitation intensity ($P_{exc} = 0.2\ W/cm^2$) is 0.39 eV. Therefore, from above inequality, we can write,

$$0.39\ eV \le \frac{1}{2}E_B \text{ or } E_B \ge 0.78\ eV \quad (4.3\text{-}3)$$

Since we don't know whether it is donor or acceptor that has the largest Bohr radius, we are going to assume both possibilities below.

First, let's assume that shallow acceptor has the largest Bohr radius. Bohr radius for Mg_{Ga} (in our case, the shallow acceptor is Mg_{Ga}) for bound hole is given as. [21]

$$R_B = \frac{\hbar}{\sqrt{2\,m_h E_A}}, \quad (4.3\text{-}4)$$

where E_A is acceptor energy with respect to valence band and $m_h = 0.8 \times m_0$, where m_0 is the mass of a free electron, is the effective mass of hole in the valence band. Bohr radius for Mg_{Ga} ($E_A = 0.2\ eV$) acceptor calculated from equation (4.3-4) is 4.88 Å.

Substituting $R_B = \frac{\hbar}{\sqrt{2\ m_h E_A}}$ in $E_B = \frac{e^2}{4\pi\epsilon_0 \epsilon R_B}$ (see section 2.3), we get

$$E_B = e^2 \frac{(2m_h E_A)^{\frac{1}{2}}}{4\pi\epsilon_0 \epsilon \hbar}. \tag{4.3-5}$$

Substituting $E_A = 0.2\ eV$ for Mg_{Ga} and $m_h = 0.8 \times m_0$, in the above equation; we get $E_B = 0.311\ eV$ and the largest expected shift is $\frac{1}{2} E_B = 0.156\ eV$.

Now let's assume that the donor has the largest Bohr radius. First, we will determine the reasonable range of E_D for this donor. For the limit of low excitation intensities ($P_{exc} \to 0$), equation (2.3-1) becomes

$$\hbar\omega_\infty = E_g - (E_D + E_A), \tag{4.3-6}$$

where $\hbar\omega_\infty$ is the emission energy or ZPL when DAP is infinitely far. Since we don't see saturation of the shift for the BL band in Fig. 4.3-1 at lowest P_{exc}, so the position of the BL band maximum at lowest P_{exc} is denoted as $\hbar\omega\ (P_{lowest})$ and can be written as

$$\hbar\omega\ (P_{lowest}) > \hbar\omega_\infty - 0.13\ eV, \tag{4.3-7}$$

where we accounted for the Frank-Condon shift between ZPL and BL max, equal to 0.13 eV. With equation (4.3-6), (4.3-7) can be written as

$$E_D > E_g - \hbar\omega\ (P_{lowest}) - E_A - 0.13\ eV, \tag{4.3-8}$$

From fig. 4.3-1, $\hbar\omega\ (P_{lowest})$ is $2.77\ eV$. Therefore, with $E_g = 3.5\ eV$ and $E_A = 0.2\ eV$, E_D can be calculated from (4.3-8) as

$$E_D > 0.4eV. \tag{4.3-9}$$

Bohr radius for the donor is given as [21]

$$R_B = \frac{\hbar}{\sqrt{2\ m_e E_D}}, \tag{4.3-10}$$

where E_D is the ionization energy of donor and $m_e = 0.2\times m_0$, where m_0 is the mass of a free electron, is the effective mass of electron in the conduction band.

For $E_D = 0.4\ eV$, the Bohr radius for donor from equation (4.3-10) would be $6.90\ \text{Å}$. Since Bohr radius is inversely proportional to the square root of ionization energy of donor, Bohr radius (R_B) for donor would be

$$R_B < 6.90\ \text{Å} \text{ for } E_D > 0.4\ eV \tag{4.3-11}$$

As the Bohr radius for shallow acceptor calculated above is $4.88\ \text{Å}$, we can't say for sure whether it is shallow acceptor or donor that has the largest Bohr radius. However, we can't take Bohr radius of donor less than $4.88\ \text{Å}$ because if we do, we would have to return to our previous assumption that shallow acceptor has the largest Bohr radius. In order to stick to our second assumption that donor has the largest Bohr radius, we will take the Bohr radius between $4.88\ \text{Å}$ and $6.90\ \text{Å}$. Donor Bohr radius of $4.88\ \text{Å}$ corresponds to $E_D = 0.8\ eV$. Hence, we should confine E_D between $0.4\ eV$ and $0.8\ eV$. i.e.

$$0.4\ eV < E_D < 0.8\ eV. \tag{4.3-12}$$

Substituting the value of R_B from equation (4.3-10) in equation $E_B = \frac{e^2}{4\pi\epsilon_0\epsilon R_B}$ (see section 2.3), E_B for donor can be written as

$$E_B = e^2 \frac{(2m_e E_d)^{\frac{1}{2}}}{4\pi\epsilon_0\epsilon\hbar}. \quad (4.3\text{-}13)$$

For $0.4\ eV < E_D < 0.8\ eV$, E_B will be in the range of $0.23 - 0.33\ eV$ and the largest possible shift will be in the range of $\frac{E_b}{2} = 0.115 - 0.165\ eV$

From both cases, we see that the observed shift $0.39\ eV$ is much larger than expected in the DAP model. Therefore, according to Zacks and Halperin, it is unlikely that shifting of the BL band in our sample is the result of saturation of PL from distant DAP due to their longer lifetime. Moreover, to have Coulomb interaction energy of $0.39\ eV$, the distance between donor and acceptor pair should be $0.39\ nm$. However, average separation (R_m) between donor and acceptor (given by $R_m = (2\pi N_A)^{-\frac{1}{3}}$, where N_A is the concentration of acceptors[16]) calculated for Mg concentration of $1.5\times10^{18}/cm^3$ in the sample is $4.73\ nm$. It is highly unlikely that such close pairs ($R < 0.4\ nm$) exist in large quantity to provide strong BL* band.

Conclusion drawn from the discussion of above two models

Once DAP model is discarded, we are left with the option of potential fluctuations in the sample to explain the shift of the BL band with excitation intensity. Potential fluctuations increase with decreasing excitation intensity facilitating diagonal transitions that shift the BL band to the lower energies. Now, the important question arises, “why don’t we see the shift of the UVL band and exciton band (Fig. 4.3-1) but only in the BL

band?" Diagonal transitions should also occur in the case of eA transition that causes UVL band if we consider the potential fluctuations in the sample.

Moreover, from Potential fluctuation model, we have also obtained the ionization energy of the deep donor (E_D) that is responsible for the BL band to be $E_D \leq (0.013 - 0.063\ eV)$. This result itself is in contradiction with the widely accepted notion that the BL band in the Mg-doped GaN is attributed to the transition between deep donor and Mg_{Ga} acceptor.[2,4,19] In our sample, it seems as if it originates from the transition between conduction band or the shallow donor and shallow Mg_{Ga} acceptor. eA transition in Mg-doped sample produces UVL band. This leads us to assume that BL band in our sample is not the BL band studied by other researchers,[2,4,19] but it is, in fact, the UVL band itself. Hence, we are going to call this band as BL^* band hereafter.

The following explanation of the above-mentioned controversies can be proposed. UVL band may originate from two regions of the sample; one region where there are no potential fluctuations and another where there are significant potential fluctuations. These two regions may exist as small domains or layers with different properties. The region without fluctuations contributes to the right part of the PL spectrum that includes UVL peak with its phonon replicas and exciton peak with its phonon replicas. Whereas, potential fluctuation region contributes to the left of the UVL band which broadens and shifts to the extent that it looks like a blue band with decreasing excitation intensity. Potential fluctuations increase with decreasing excitation intensity facilitating diagonal transitions that shift the band to lower energies. The presence of many diagonal transitions with different vertical components also helps the band to broaden with decreasing excitation intensity.

The reasonable answer for why we don't see usual BL band in our Mg-doped sample could be that there are not many competitive deep donors that are generally introduced while Mg is doped in the sample and which are responsible for the usual BL band. Besides, the concentration of the Mg acceptors is too low, so that overlap of wavefunctions of holes bound to shallow Mg_{Ga} acceptors and electrons bound to unknown deep donors is too small. Then, the intensity of related BL band is expected to be very low.

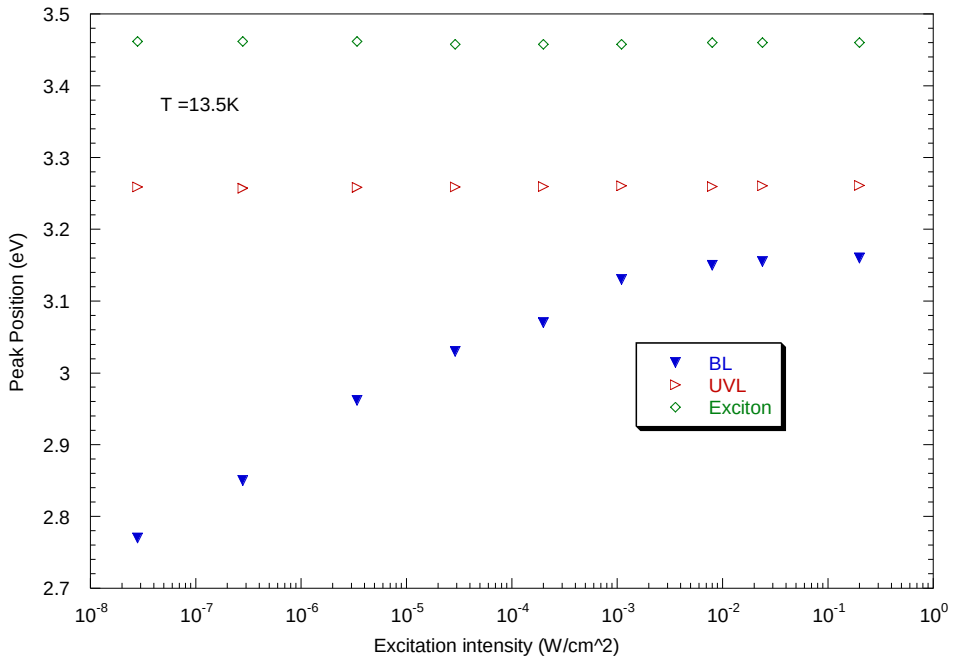

Fig 4.3-1: Peak positions of BL, UVL and exciton band with respect to excitation intensities.

4.4 Dependence on temperature

PL spectra of Zn-doped and Mg-doped GaN have shown very interesting phenomena with changing temperature. Abrupt and tunable thermal quenching of photoluminescence had been observed by increasing temperature for the blue, Zn-related BL band in high-resistivity Zn-doped GaN.[13] Almost same kind of behavior was also observed for the UVL band with a maximum about $3.25\ eV$ in Mg-doped GaN.[14] By finding the slope of a graph of the inverse of characteristic temperature (temperature at which quenching begins) for the BL band (in case of Zn-doped GaN) and for UVL band (in case of Mg-doped GaN) as a function of the generation rate, the ionization energy of the shallow acceptor that caused quenching was determined.

Figs. 4.1-2 (a)-(e) show the evolution of PL spectra with temperature for a fixed laser intensity. Below, the dependence of PL intensity and PL peak positions on temperature are discussed in detail.

i) PL Intensity

PL spectra shown in Figs. 4.1-2 (a)-(e) have mainly Exciton, UVL, and BL bands. The features of these bands and some distinguishable changes with temperature are explained below.

Exciton band has three main peaks. The first peak at $3.467\ eV$ is due to exciton bound to Mg_{Ga} acceptor (ABE). The second peak at $3.471\ eV$ is attributed to donor bound exciton (DBE). The third peak at $3.479\ eV$ (at $13.5\ K$) is due to the annihilation of the free exciton. ABE peak is accompanied by LO phonon replica at $3.375\ eV$. For

$P_{exc} = 0.2\ W/cm^2$, ABE peak disappears at temperatures above $40\ K$, and the whole exciton band is dominated by DBE up to about $90\ K$ and by free excitons above $90\ K$. Free exciton peak shifts to lower energy by about $23\ meV$ in the temperature range of $13.5\ K$ to $180\ K$. With increase in temperature, exciton peak intensity decreases until $190\ K$ for $P_{exc} = 0.2\ W/cm^2$ and it starts increasing above $190\ K$. This temperature at which exciton peak starts to increase decreases with excitation intensity. Moreover, exciton band after this turning temperature point doesn't actually look like a usual exciton band, which is a mystery.

UVL band is the dominant defect-related band in the spectrum at low temperature and high excitation intensity. It has the first peak at $3.267\ eV$ followed by three phonon replicas (the third one appears as a shoulder even at $P_{exc} = 0.2\ W/cm^2$ and $T = 13.5\ K$) at $3.177\ eV$, $3.087\ eV$, and $2.997\ eV$. With increasing temperature, UVL peak intensity decreases and broadens on the left portion of the band for $P_{exc} = 0.2\ W/cm^2$ and turns into a band which we identify as BL* band, better resolved at lower excitation intensities. In section 4.3, we proposed that this band could be the UVL band itself, but arising from the regions of the sample where potential fluctuations are dominant.

The BL* band starts appearing with increase in temperature. At low temperature, UVL is dominant in the spectrum. The contribution of the BL* band in the spectrum was obtained by the deconvolution method. The peak intensity of the BL* band remains almost fixed or slightly decreases for low temperatures and starts dropping gradually at higher temperatures (Figs. 4.1-2 (a) and (b)). This gradual drop becomes abrupt at lower excitation intensities (Figs. 4.1-2 (c), (d) and (e)).

a) Temperature dependence of the exciton peak intensity

Temperature dependence of peak intensity of Exciton band is shown in Fig. 4.4-1 (a). Intensity decreases slowly as the temperature increases up to about $100\,K$. However, we observe abrupt drop after the temperature reaches a certain level. The temperature T_0 at which the drop becomes abrupt is called the characteristic temperature. It increases with increasing excitation intensity (Fig. 4.4-1 (a) and Fig. 4.4-4(a)). Solid lines in the Fig. 4.4-1 (a) are the fit to the equation [22]

$$I = \frac{I_0}{1 + c\, e^{-\frac{E}{KT}}}, \tag{4.4-1}$$

where, I_0 is the low-temperature intensity of exciton peak, E is the activation energy of exciton and c is a constant. From this fit, the activation energy of exciton is $14\,meV$ for all excitation intensities. However, the slope of quenching at $T > T_0$ is $50 - 105\,meV$, much larger than the activation energy of $14\,meV$. Characteristic temperature (T_0) of quenching of exciton band in Fig. 4.4-1 (a) (shown for $P_{exc} = 0.2\,W/cm^2$) was found by the intersection of extrapolation of abruptly quenched part with the fit given by Eq. (4.4-1).

The ionization energy of shallow acceptor which causes the abrupt quenching of a PL band by thermally emitting holes to the valence band, thereby triggering a sudden opening of the nonradiative channel, can be found by plotting the inverse of characteristic temperature of PL quenching as a function of the generation of electron-hole pair.[13] The inverse of characteristic temperatures (T_0) of exciton band (obtained from Fig. 4.4-1 (a)) is plotted against the logarithm of generation rate (G) of free electron and hole pair in Fig. 4.4-4 (a). Solid line in the figure is the fit to the equation of (2.4-1) [13]

$$T_0 = \frac{E_A}{k \ln(B/G)}. \quad (2.4\text{-}1)$$

Here, E_A is the ionization energy of the acceptor responsible for abrupt quenching, k is Boltzmann's constant, G is the generation rate of electron-hole pairs and B is a constant which depends on hole capture coefficient, low-temperature quantum efficiency of PL through acceptor A, concentration of defects and effective density of states in the valence band.

From the fit of equation (2.4-1) in the plot of Fig. 4.4-4 (a), the ionization energy of the acceptor (E_A) responsible for abrupt quenching was found to be $240\ meV$, close to the shallow acceptor energy.

b) Temperature dependence of the UVL peak intensity

UVL band intensity remains almost constant with temperature (at high excitation intensities) and slowly decreases (at low excitation intensities) up to certain temperature after which it starts quenching with an activation energy of $100 - 125\ meV$ as shown in Fig. 4.4-1 (b). The characteristic temperature (T_0) at which the quenching begins is obtained from the intersection of extrapolation of low temperature ($T < T_0$) portion and high temperature ($T > T_0$) portion. The inverse of characteristic temperature (T_0) of the UVL band is plotted against the generation rate (G) in Fig. 4.4-4 (b). The solid line in the figure is fit to the Eq. (2.4-1). Although UVL band doesn't quench abruptly, a linear dependence of inverse of characteristic temperature (T_0) on logarithm of generation rate (G) shows that quenching is tunable.

The ionization energy of the acceptor responsible for quenching of the UVL band in Mg-doped GaN grown by MBE had been found to be $250 - 270\ meV$.[14] In our sample, we obtained it to be $250\ meV$ which is close to the ionization energy of $150 - 200\ meV$ of Mg_{Ga} acceptor found in the literature.[16]

c) Temperature dependence of the BL* peak intensity

Unlike Exciton and UVL bands, temperature dependence of the BL* band peak intensity looks different for high excitation intensity and low excitation intensity. Fig. 4.4-1 (c) shows the temperature dependence of BL* band peak intensity. As can be seen in the figure, intensity decreases with temperature slowly (not abruptly) for excitation intensity, $P_{exc} \geq 0.0011\ W/cm^2$. The activation energy of quenching for $P_{exc} \geq 0.0011\ W/cm^2$ was found to be $95 - 150\ meV$. However, intensity abruptly drops at characteristic temperature (T_0) for $P_{exc} \leq 0.0002\ W/cm^2$.

Characteristic temperature at which the quenching begins was obtained from the intersection of extrapolation of low temperature ($T < T_0$) portion and the abruptly quenched part in Fig. 4.4-1 (c). The inverse of characteristic temperatures (T_0) of the BL* band is plotted against the generation rate (G) in Fig. 4.4-4 (c). This plot was fitted with equation (2.4-1). From the fit, the ionization energy of acceptor (E_A) responsible for quenching was found to be 240 meV.

It's quite unusual for the same band to exhibit abrupt and tunable thermal quenching at low excitation intensities and "normal" quenching at higher excitation intensities. To check the reproducibility of the measurements, sample was removed from the cryostat and kept in air for about 25 days and then it was again placed in the

cryostat and the experiment was repeated for $P_{exc} = 3.4\times10^{-6}\, W/cm^2$ during several days under continuous vacuum condition. Fig. 4.4-2 (a) shows the graph of BL* band intensity vs. inverse of temperature taken at various days after storing the sample for 25 days in air. From the figure, we can compare the result obtained (on 5/31/2016) when the sample was kept in vacuum for 13 days in the first installation with the results obtained in the second installation after the sample was exposed to air for 25 days. After exposure, at the first day (7/5/2016) of the second installation, the quenching didn't match at all the result of 5/31/2016. The intensity drop is quite slow compared to the abrupt drop on 5/31/2016. However, as the time increases, or, in other words, when the amount of time sample remains in vacuum increases, the drop of the intensity becomes more and more abrupt. After 13 days in vacuum (on 7/18/2016), it appears that the drop is about the same abrupt as the one obtained on 5/31/2016.

The different behavior of intensity of BL* band with temperature when the sample is in vacuum and after it is exposed to air indicates that intensity of BL* band depends on the environmental effects on the sample. Figs. 4.4-2 (b)-(d) also show the BL* intensity vs. inverse of temperature for different excitation intensities taken after different time in vacuum. Temperature dependence of the BL* band intensity measured on 5/26/2016 (8 days in vacuum on the first installation) and 7/19/2016 (14 days in vacuum on the second installation) for $P_{exc} = 2.9\times10^{-5} W/cm^2$ do not match as shown in Fig. 4.4-2 (b). Fig. 4.4-2 (c) shows temperature dependence of the BL* band intensity measured on 5/25/2016 (7 days in vacuum on the first installation) and 7/19/2016 (14 days in vacuum on the second installation) for $P_{exc} = 0.0002 W/cm^2$. It is clear from the Fig. 4.4-2 (c) that BL* band doesn't fully restore its quenching behavior. However, for

high excitation intensity ($P_{exc} = 0.0002 W/cm^2$), temperature dependence of BL* band peak intensity measured on 5/24/2016 (6 days in vacuum on the first installation) matches with the result measured on 7/20/2016 (15 days in vacuum on the second installation) as shown in Fig. 4.4-2 (d). In conclusion, it can be conjectured that the temperature dependence of BL* band at high excitation intensity is independent of ambient but it is ambient-dependent at low excitation intensities.

Interestingly, at the same time, UVL band doesn't look to be affected by environmental conditions. Fig. 4.4-3 (a) shows the temperature dependence of the UVL peak intensity obtained at different environmental conditions for $P_{exc} = 3.4\times 10^{-6}\, W/cm^2$. Curves in the figure are named in a way that indicates when they were measured. For example, curve "5/31/2016" was plotted for the experiment done on 5/31/2016 after the sample was kept in vacuum for 13 days. Sample was first installed on 5/18/2016. Curve "7/5/2016" was taken at the first day (7/5/2016) of second installation after sample was exposed to air for 25 days. All other curves are taken (after the second installation of the sample) on the days that match with their names. Unlike temperature dependence of the BL* peak intensity in Fig. 4.4-2, temperature dependence of the UVL peak intensity is almost the same irrespective of the days measured and environmental conditions imposed. Figs. 4.4-3 (b), (c) and (d) also show the temperature dependence of the UVL peak intensity measured on different days. These curves (for fixed excitation intensity) in different figures also match with each other. This further supports our conclusion that temperature dependence of the UVL peak intensity is independent of the time of measurement and outside environment.

Different types of temperature dependence of the BL* peak intensity and the UVL peak intensity agrees with our previous assumption that the BL* band and the UVL band might have come from different regions of the samples. The regions from where the BL* band comes most likely get affected by environmental conditions imposed. However, the regions from where the UVL band comes are not affected by outside environment. This leads us to assume that BL* band comes from the near surface region of the sample, whereas, UVL band comes from bulk region of the sample. In Sec. 4.3, we proposed that potential fluctuations in the region where BL* band comes from, are the main reason behind the blueshifting of the band with increasing excitation intensity. However, now we have a convincing reason to believe that the BL* band comes from the near surface reason, we must see the possibility of band bending at the surface of GaN where all potentials are bent upward for n-type GaN and downwards for p-type GaN (Fig. 4.4-6).[23,24,25]

Band bending (upward or downward) arise due to the surface charge (negative or positive) which may originate from defects at the surface such as dangling bonds, lattice mismatch, impurities or absorbed species.[26] $1\ eV$ of band bending in n-type [25] and $2\ eV$ of band bending in p-type GaN [27] have been calculated for dark conditions. The magnitude of band bending decreases with increasing excitation intensity. Once the sample is illuminated, electron-hole pairs are generated. Electrons move to the surface of p-type material and to the bulk of n-type material. Opposite is the case for holes. This reduces the overall surface charge almost instantly, leading to the reduction in magnitude of the band bending. When there is a significant band bending in the surface region, diagonal transitions are facilitated giving rise to a PL of low energy. Once band

bending decreases with excitation intensity, transitions become more vertical leading to the PL emission of higher energy.

II) BL* band peak position

Dependence of BL* peak position on temperature is shown in Fig. 4.4-5. Plot for high excitation intensity starts at higher position than lower excitation intensity in the figure indicating that BL* band blueshifts with increasing excitation intensity. This is in tune with what we saw in section 4.3 where we discussed that potential fluctuations is the reason behind the blueshift of this band with excitation intensity. For excitation intensities, between 0.0011 to $0.2\ W/cm^2$, BL* band redshifts slowly after some critical temperature (T^*). For $P_{exc} \leq 0.0002\,W/cm^2$, redshift at $T > T^*$ becomes very quick. Critical temperature (T^*) is the temperature at which band shift becomes more pronounced. We cannot say a priory if it is equal to the characteristic temperature (T_0) discussed in PL quenching or not. BL* positions are almost fixed before critical temperature is reached for $P_{exc} \geq 2.87\times10^{-5}\,W/cm^2$. However, BL* band redshifts slowly even before critical temperature is reached for $P_{exc} < 2.87\times10^{-5}\,W/cm^2$. Note that giant shift at $T > T^*$ is observed for the same excitation intensities ($P_{exc} \leq 0.0002\,W/cm^2$) where the abrupt and tunable quenching is observed at $T > T_0$, compare with Fig. 4.4-1 (c).

Red shift of the BL* band in our sample can be explained by the combined effect of potential fluctuations in the sample and abrupt tunable thermal quenching of BL* band. As we have already discussed in section 4.3, potential fluctuations are present in the region of the sample where BL* band comes from. Electrons and holes in the conduction and valence bands always try to occupy the minimum energy states. Minimum energy state for electrons in the conduction band is the potential well, while it is potential hill for holes in the valence band. When electrons and holes are

accumulated at potential wells and hills, they tend to flatten the potentials of the system. In other words, they decrease the fluctuations. As temperature increases and approaches T^*, electrons and holes get enough energy to overcome potential barriers around wells and hills and travel through the band. This increases the fluctuations as electrons and holes are not accumulated to neutralize the effect of randomly distributed charged defects which causes fluctuations. Increased fluctuations facilitate more diagonal transitions with reduced emission energy. Hence the band is red shifted.

Moreover, electrons which are in a local minimum of the conduction band may not be in the absolute minimum position. Once an electron gets enough thermal energy it may overcome the barrier of that well where it was residing and move to the potential well of further minimum level. Now when the electrons are in much deeper well, the transition from that well to the Mg_{Ga} acceptor will produce the PL of smaller energy due to diagonal transitions than it would produce when electrons were in elevated minima. Thus, the band is red shifted.

The above mechanisms cannot alone explain the giant shift of the BL* peak position observed at low excitation intensities ($P_{exc} \leq 0.0002\, W/cm^2$). At these low excitation intensities, the temperatures at which the quenching of PL begins (T_0) and the giant shift begins (T^*) are almost the same (see Fig. 4.4-7). This information hints us to consider abrupt quenching of the BL* band that we discussed in Sec. 4.4 (I) as the possible cause for the observed giant shift.

At low temperature ($T < T_0$), after illumination, nonradiative S-centers are saturated with electrons. As a result, there will be an accumulation of electrons in the

conduction band.[13] At ($T \approx T_0$), holes at the shallow Mg_{Ga} acceptors get enough thermal energy to be thermally emitted to the valence band. These holes at the valence band now efficiently recombine with electrons at the S-centers nonradiatively, causing the sudden drop of electrons in the conduction band. Fig. 4.4-8 shows an example of calculations, according to which, at critical temperature (T_0), the concentration of free electrons in the conduction band drops substantially by more than three orders of magnitude. This abrupt decrease in concentration of electrons in the conduction band causes the potential fluctuations to increase sharply (explained in detail in Sec. 2.2 and Sec.4.3). With the sharp increase in potential fluctuations, BL* band shifts greatly to lower energy as more diagonal transitions are facilitated.

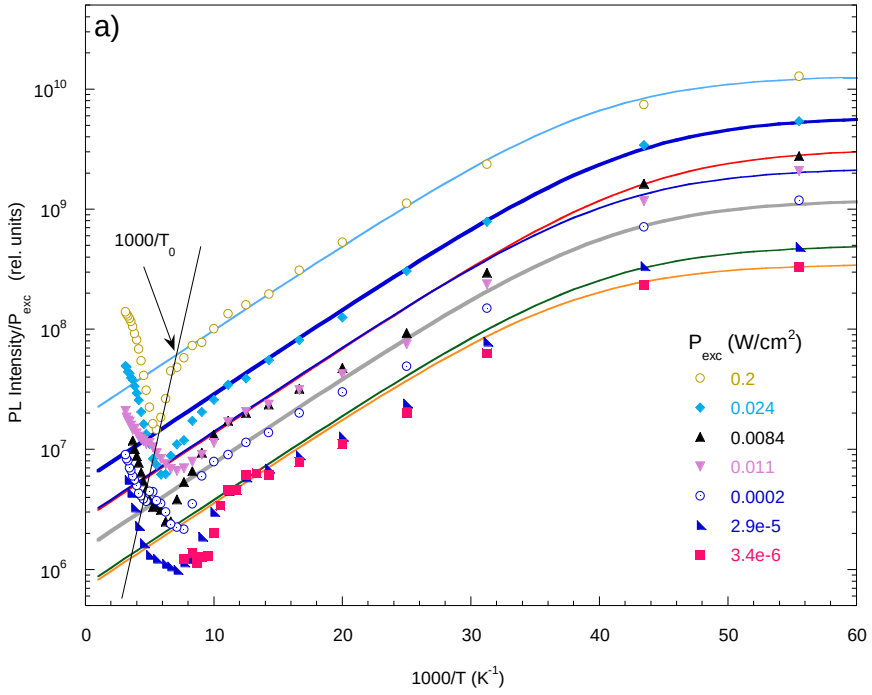

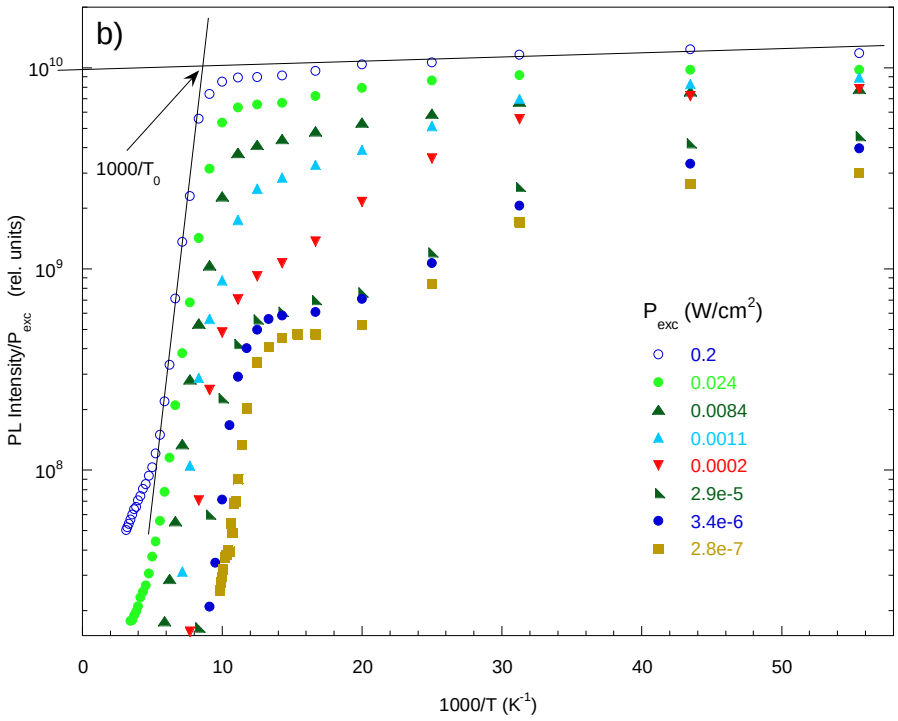
b)
10^{10}
10^{9}
10^{8}
1000/T_0
PL Intensity/P_{exc} (rel. units)
P_{exc} (W/cm^2)
0.2
0.024
0.0084
0.0011
0.0002
2.9e-5
3.4e-6
2.8e-7
0
10
20
30
40
50
1000/T (K^{-1})

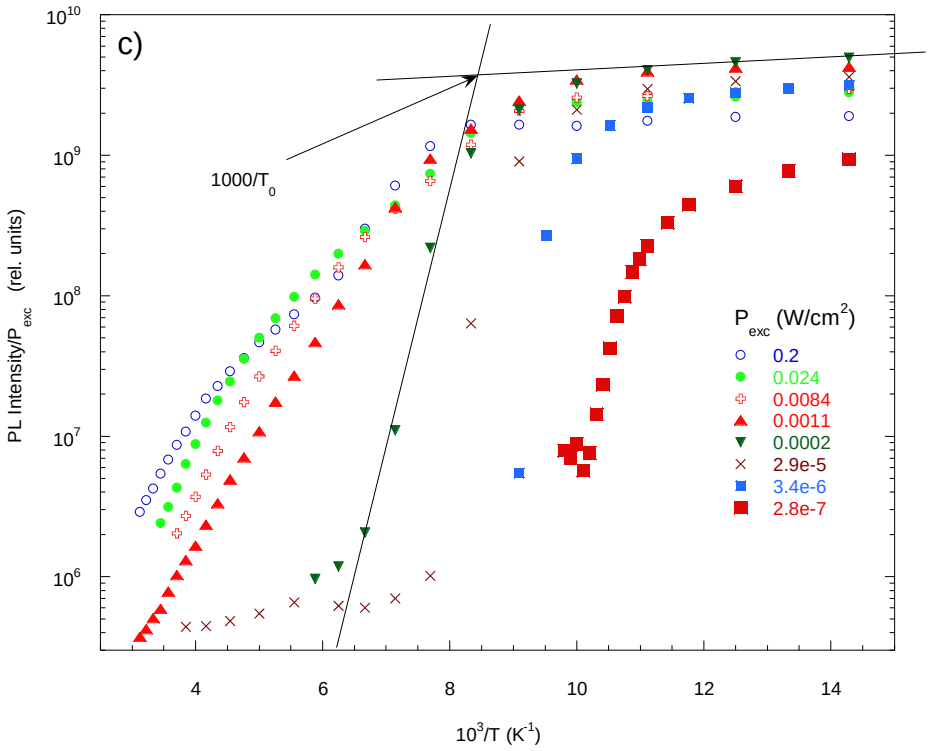

Fig: 4.4-1: Temperature dependence of the peak intensity of various bands; a) exciton b) UVL and c) BL band. T_0 is indicated for the highest excitation intensity as the intersection of extrapolation of low-temperature region ($T < T_0$) and quenched region ($T > T_0$).

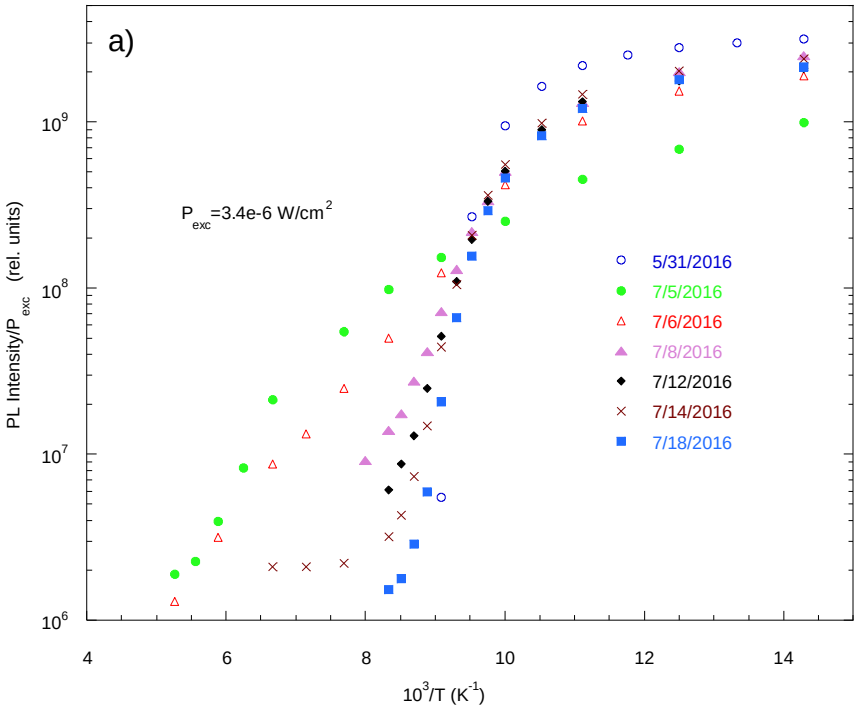
a)
P_exc=3.4e-6 W/cm^2
5/31/2016
7/5/2016
7/6/2016
7/8/2016
7/12/2016
7/14/2016
7/18/2016
PL Intensity/P_exc (rel. units)
10^3/T (K^-1)

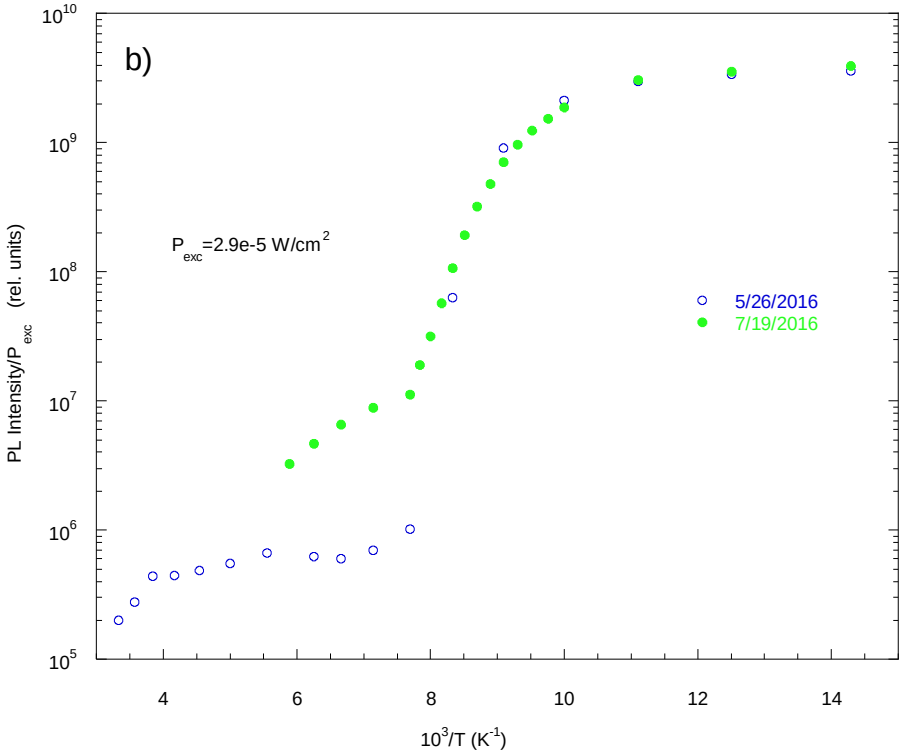
b)
P_exc=2.9e-5 W/cm^2
5/26/2016
7/19/2016
PL Intensity/P_exc (rel. units)
10^3/T (K^-1)

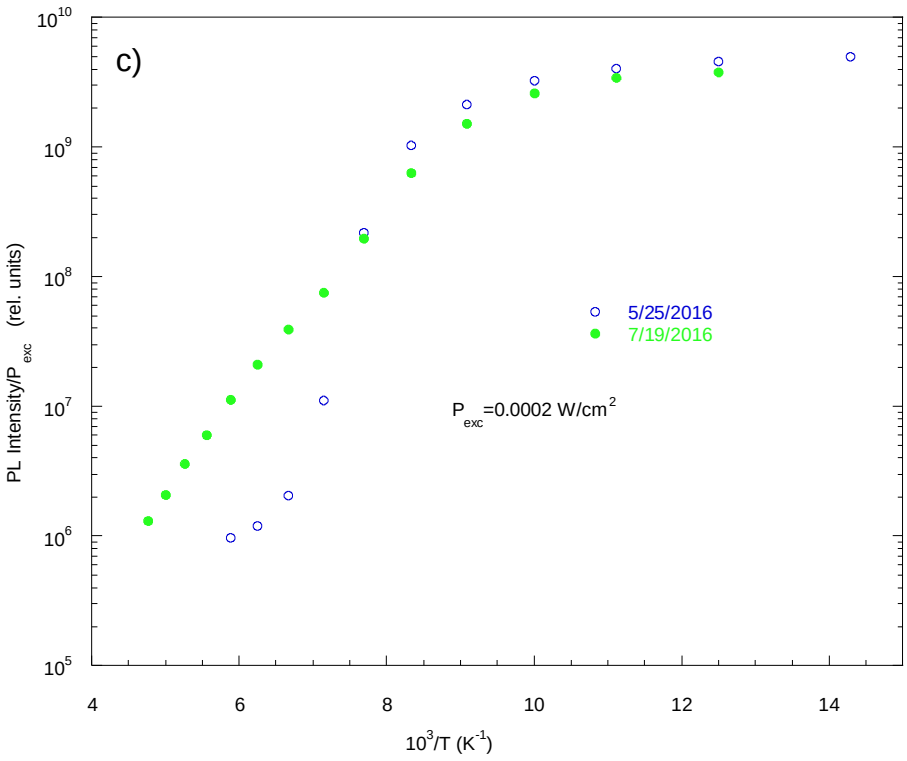
c)
PL Intensity/P_exc (rel. units)
10^10
10^9
10^8
10^7
10^6
10^5
4
6
8
10
12
14
10^3/T (K^-1)
5/25/2016
7/19/2016
P_exc=0.0002 W/cm^2

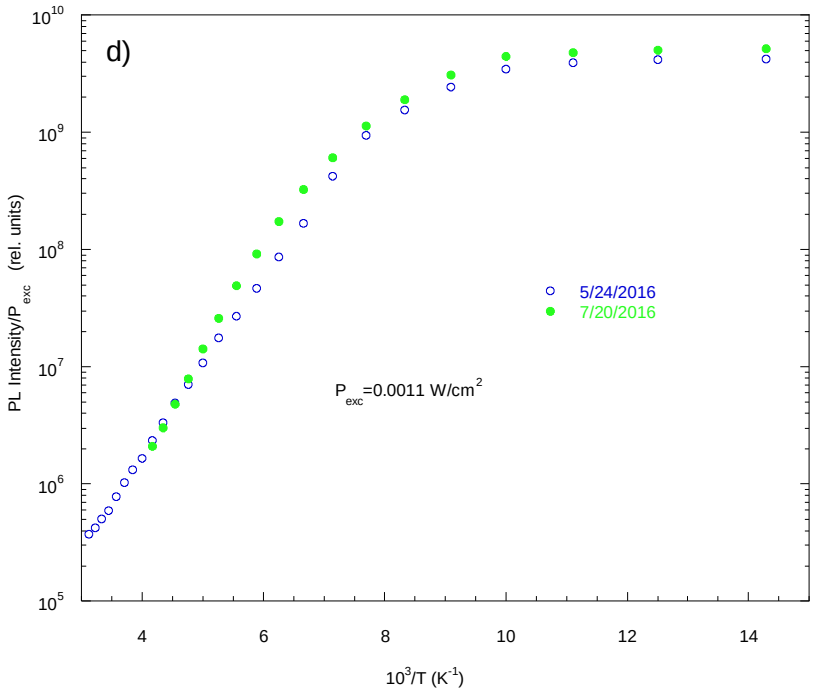

Fig. 4.4-2: Temperature dependence of BL peak intensity measured at different days for fixed excitation intensity. For all the figures, name of the curve is kept for simplicity as the date of the experiment. For example, curve "5/31/2016" is measured on 5/31/2016. (a) Curve "5/31/2016" was obtained after the sample was kept in vacuum for 13 days. It is unknown how long the sample was exposed to air before its first installation on 5/18/2016. Curve "7/5/2016" was obtained at the first day of experiment on the second installation on 7/5/2016 after it was exposed to air for 25 days. All other curves are obtained on the days mentioned on the figure after the second installation of the sample 7/5/2016. $P_{exc} = 3.4\times10^{-6}\ W/cm^2$*. As the day progresses, Quenching of the BL* band intensity obtained after exposure to air for 25 days approaches the quenching obtained after the sample was kept in vacuum for 13 days i.e., "5/31/2016" (b) Curve "5/26/2016" was obtained after 8 days on vacuum of the first installation. Curve "7/19/2016" was obtained after 14 days on vacuum of the second installation.* $P_{exc} = 2.9\times10^{-5}\ W/cm^2$*. (c) Curve "5/25/2016" was obtained after 7 days on vacuum of the first installation. Curve "7/19/2016" was obtained after 14 days on vacuum of the second installation.* $P_{exc} = 0.0002\ W/cm^2$*. (d) Curve "5/24/2016" was obtained after 6 days on vacuum of the first installation. Curve "7/20/2016" was obtained after 15 days on vacuum of the second installation.* $P_{exc} = 0.0011\ W/cm^2$*. Two curves obtained on two different days and condition for (b) and (c) doesn't match but they fairly match for (d).*

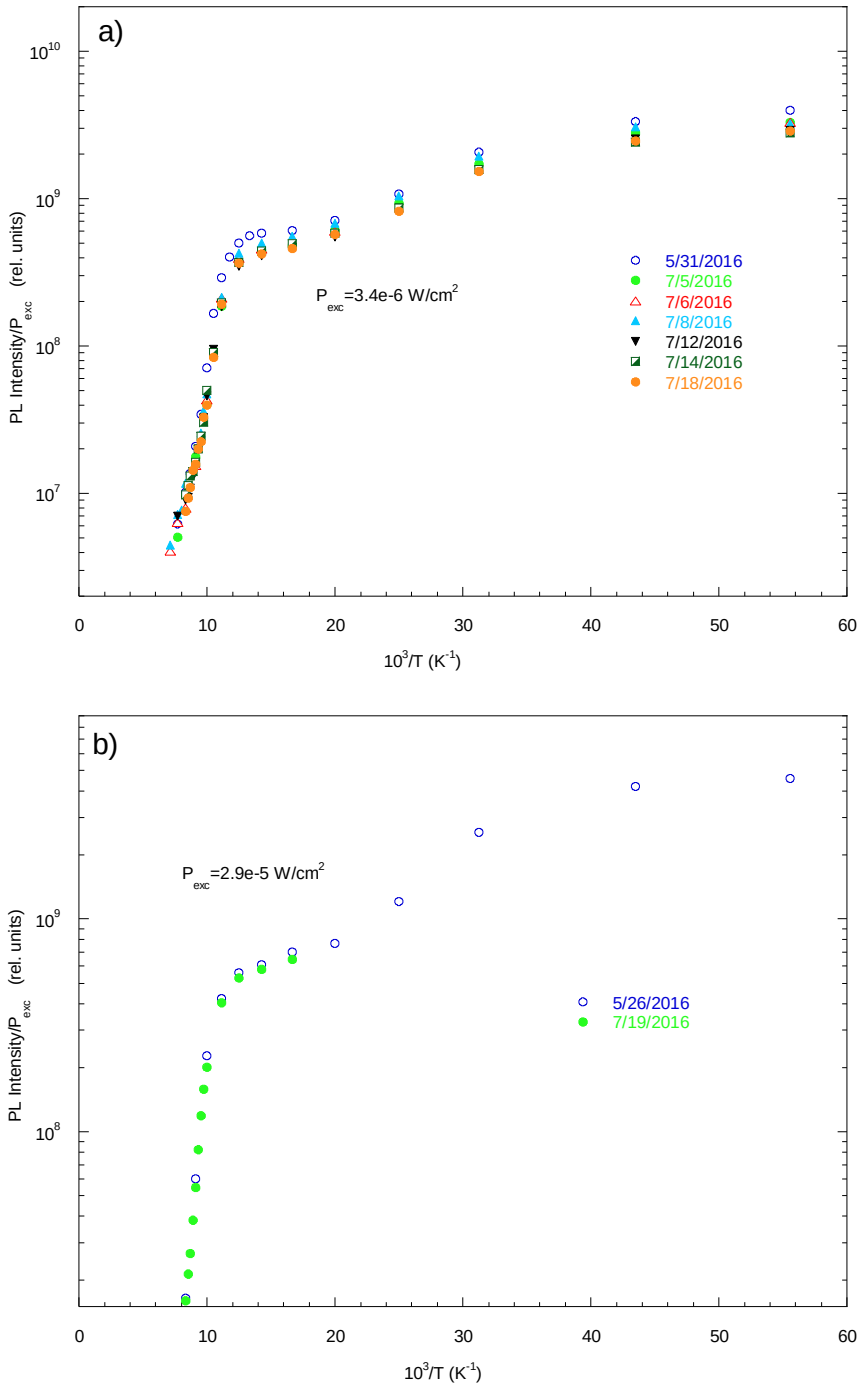
a)
PL Intensity/P_exc (rel. units)
10^10
10^9
10^8
10^7
P_exc=3.4e-6 W/cm^2
5/31/2016
7/5/2016
7/6/2016
7/8/2016
7/12/2016
7/14/2016
7/18/2016
0
10
20
30
40
50
60
10^3/T (K^-1)
b)
PL Intensity/P_exc (rel. units)
10^9
10^8
P_exc=2.9e-5 W/cm^2
5/26/2016
7/19/2016
0
10
20
30
40
50
60
10^3/T (K^-1)

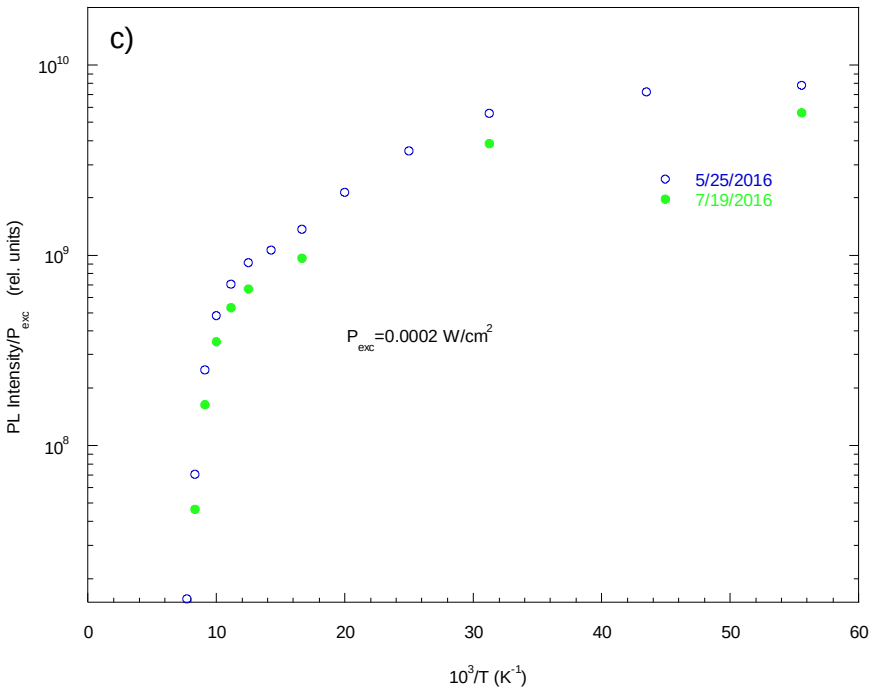
c)
10^{10}
10^{9}
10^{8}
PL Intensity/P_{exc} (rel. units)
5/25/2016
7/19/2016
P_{exc}=0.0002 W/cm^2
0
10
20
30
40
50
60
10^3/T (K^{-1})

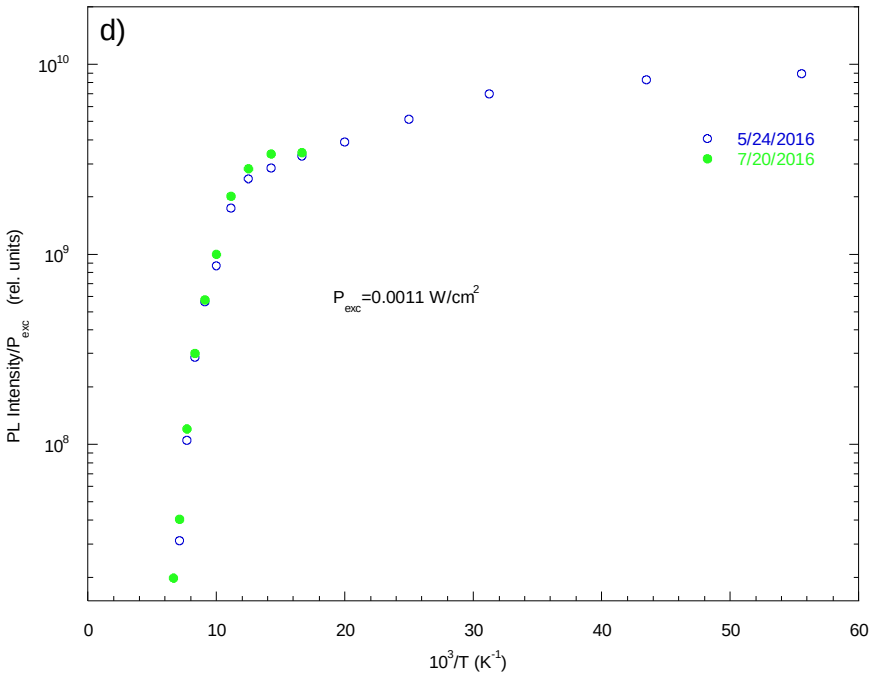

Fig. 4.4-3: Temperature dependence of the UVL peak intensity measured at different days for fixed excitation intensity. For all the figures, name of the curve is kept for simplicity as the date of the experiment. For example, curve "5/31/2016" is measured on 5/31/2016. (a) Curve "5/31/2016" was obtained after the sample was kept in vacuum for 13 days. It is unknown how long the sample was exposed to air before its first installation on 5/18/2016. Curve "7/5/2016" was obtained at the first day of experiment on the second installation on 7/5/2016 after it was exposed to air for 25 days. All other curves are obtained on the days mentioned on the figure after the second installation of the sample on 7/5/2016. $P_{exc} = 3.4\times10^{-6}\ W/cm^2$*. All curves almost match each other indicating that thermal quenching of the UVL band doesn't depend on the outside environment. (b) Curve "5/26/2016" was obtained after 8 days on vacuum of the first installation. Curve "7/19/2016" was obtained after 14 days on vacuum of the second installation.* $P_{exc} = 2.9\times10^{-5}\ W/cm^2$*. Both curves match each other. (c) Curve "5/25/2016" was obtained after 7 days on vacuum of the first installation. Curve "7/19/2016" was obtained after 14 days on vacuum of the second installation.* $P_{exc} = 0.0002\ W/cm^2$*. Both curves fairly match each other (d) Curve "5/24/2016" was obtained after 6 days on vacuum of the first installation. Curve "7/20/2016" was obtained after 15 days on vacuum of the second installation.* $P_{exc} = 0.0011\ W/cm^2$*. Here also, both curves match each other.*

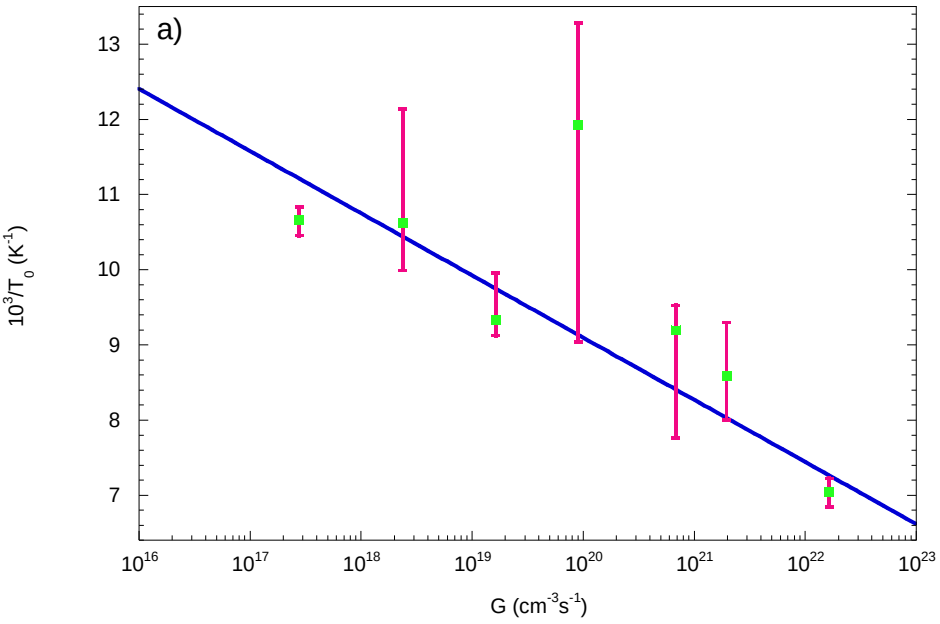
a)
13
12
11
10
9
8
7
$10^3/T_0$ (K^{-1})
10^{16}
10^{17}
10^{18}
10^{19}
10^{20}
10^{21}
10^{22}
10^{23}
G ($cm^{-3}s^{-1}$)

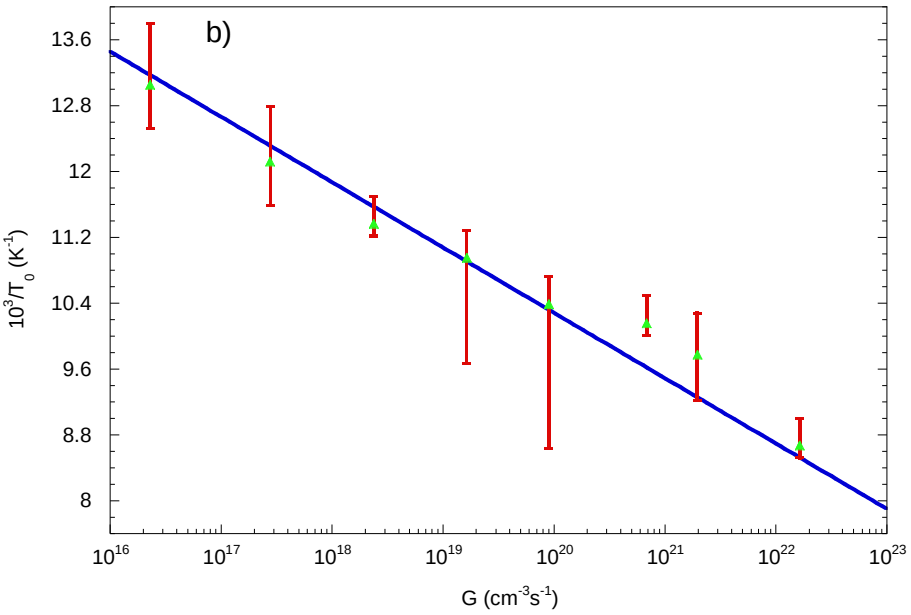
b)
13.6
12.8
12
11.2
10.4
9.6
8.8
8
$10^3/T_0$ (K^{-1})
10^{16}
10^{17}
10^{18}
10^{19}
10^{20}
10^{21}
10^{22}
10^{23}
G ($cm^{-3}s^{-1}$)

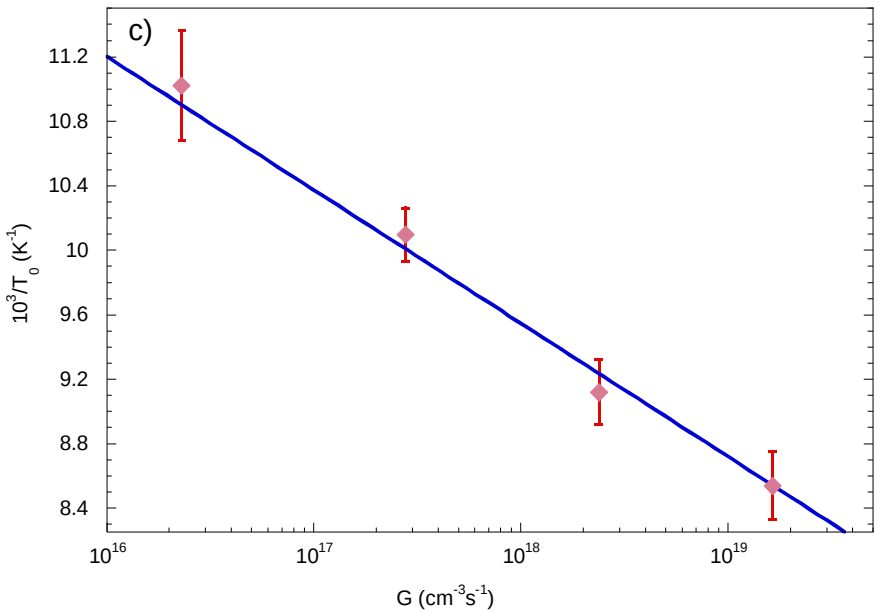

Fig: 4.4-4: Dependence of characteristic temperature T_0 on generation rate for the PL bands: a) Exciton b) UVL and c) BL. Characteristic temperatures of the BL band is plotted only for $P_{exc} \leq 0.0002\, W/cm^2$ because for higher excitation intensities BL band doesn't show abrupt quenching. The solid line is the fit to the Eq. (4.4-2) with a) $E_A = 240\, meV$ and $B = 1\times10^{31} cm^{-3}s^{-1}$. b) $E_A = 250\, meV$ and $B = 9\times10^{32} cm^{-3}s^{-1}$. c) $E_A = 240\, meV$ and $B = 3.5\times10^{29} cm^{-3}s^{-1}$.

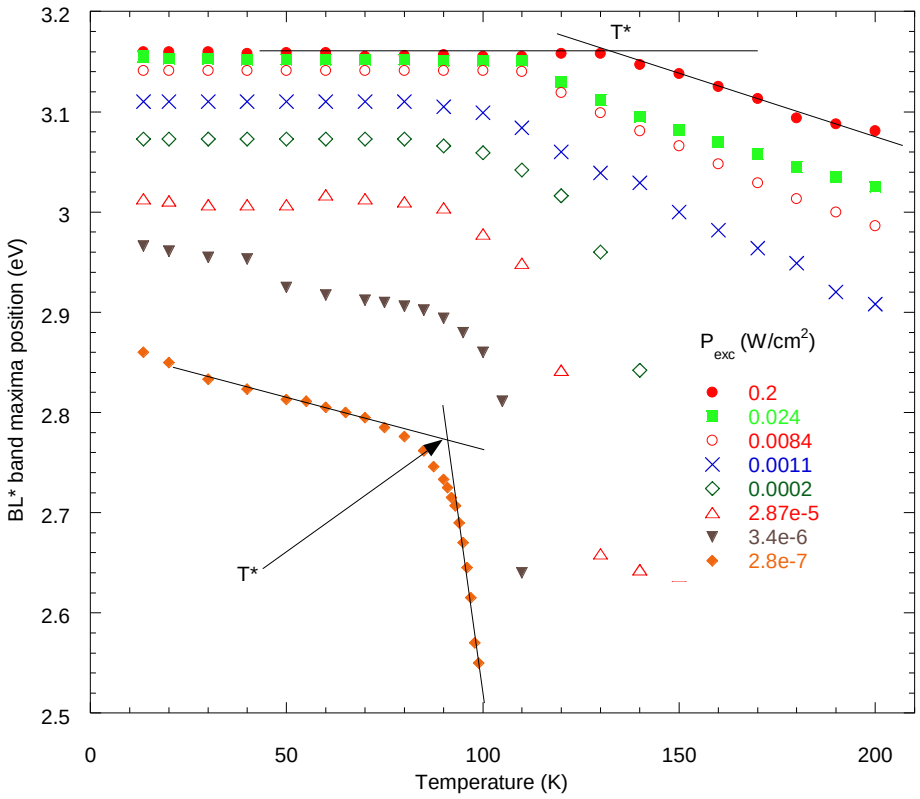

Fig. 4.4-5: Temperature dependence of the BL band*

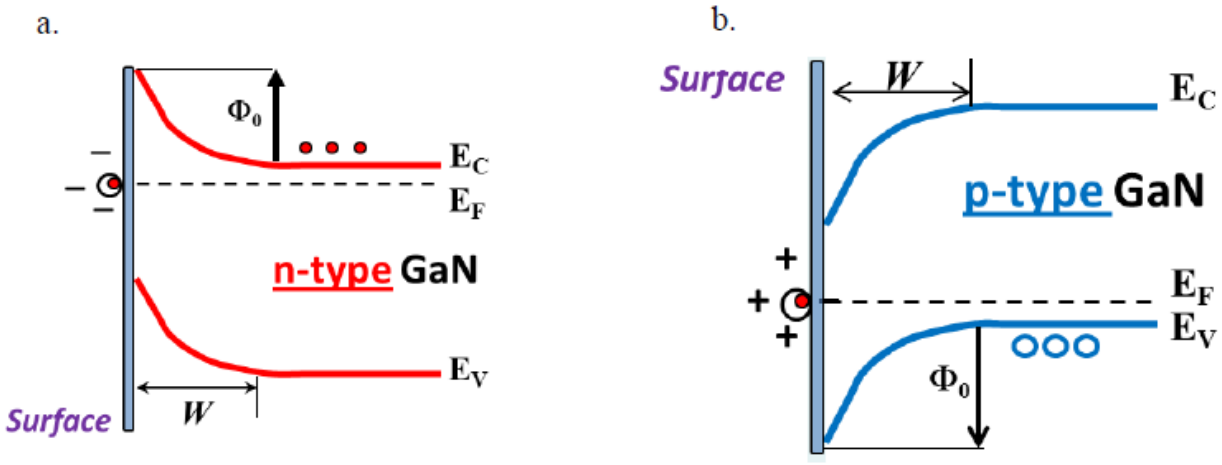

Fig. 4.4-6: Energy band diagrams for (a) n-type and (b) p-type GaN. The band bending in dark is indicated by Φ_0, the depletion region by W, and the energy levels of the conduction band, electron Fermi level and valence band by E_C, E_F and E_W, respectively. The band bending is caused by negative and positive charge at the surface, respectively. (Figures and caption by the courtesy of Joy McNamara)

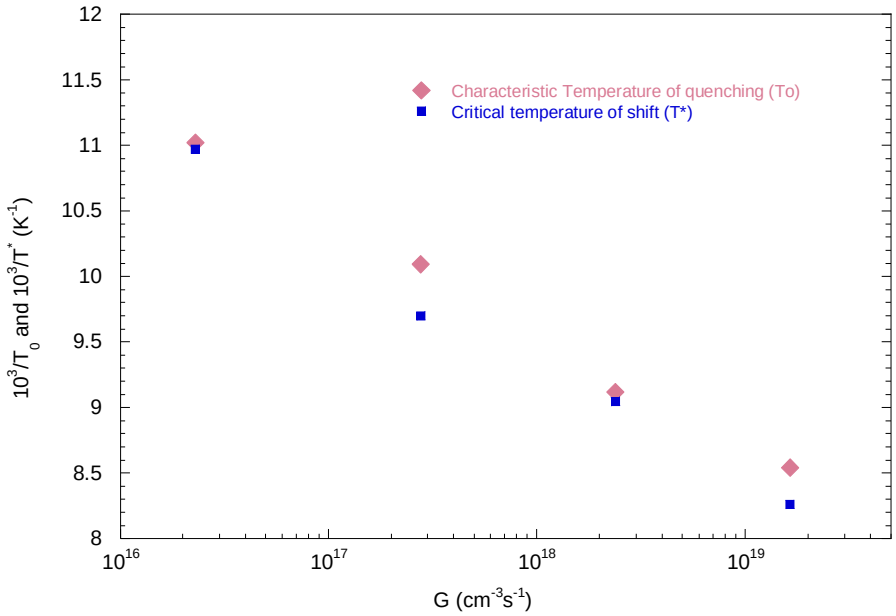

Fig. 4.4-7: Dependence of inverse of characteristic temperature (T_0) of quenching and critical temperature (T^*) of the shift of the BL band on generation rate (G) for $P_{exc} \leq 0.0002\, W/cm^2$. Note that T_0 and T^* almost match.*

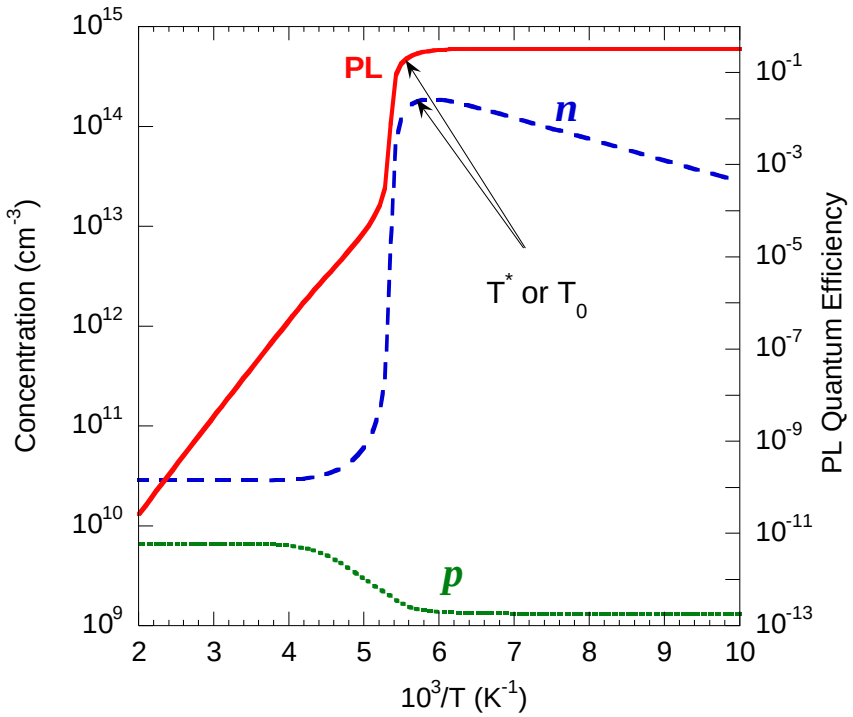

Fig. 4.4-8: Calculated dependence of PL quantum efficiency and concentration of electrons and holes in the conduction and valence bands respectively with temperature. The concentration of electrons decreases by more than three orders of magnitude at the characteristic temperature at which the PL band starts quenching abruptly. Concentration of holes in the valence band increases but it is too small compared with the decrease in concentration of electrons in the conduction band. The simulation is for Zn in GaN, after Ref. [13].

5. Conclusions

We studied HVPE grown Mg-doped GaN by the method of steady-state photoluminescence. PL spectra were obtained at various excitation intensities while keeping the temperature ($T = 13.5\,K$) fixed. Similarly, PL spectra were obtained at various temperatures keeping the excitation intensity fixed.

Excitation intensity dependence of peak positions for dominant PL bands (namely, Exciton, UVL and BL bands) were analyzed. Exciton and UVL bands show almost no shift with excitation intensity, but the BL band shows a blueshift of $\sim 0.4\,eV$ with increasing excitation intensity by seven orders of magnitude. The shift of the BL band to low energy with decreasing excitation intensity was explained by significant potential fluctuations in the sample. Potential fluctuations which increase with decreasing excitation intensity, facilitate diagonal transitions of electrons, from the conduction band to acceptors responsible for the origin of the band. Hence, the band shifts to lower energy with decreasing excitation intensity. All the results could be explained only in an assumption that the sample is not uniform, but consists of domains with different properties. In particular, the constant band position of the UVL and exciton bands with excitation intensity was explained by assuming that UVL and exciton bands originate from the regions of the sample where potential fluctuations are not present. Since BL band in literature is commonly attributed to transitions between a deep donor and shallow Mg_{Ga} acceptor in GaN heavily doped with Mg**,** we also looked at the possibility of saturation of distant donor-acceptor pairs with excitation intensity due to their longer life-time to explain the significant blueshift of the BL band with increasing

excitation intensity. From the study of both potential fluctuations model and DAP model, we came to a conclusion that BL band in our sample doesn't originate from the transition between deep donor and Mg_{Ga} acceptor, rather it comes from the transition between shallow donor and Mg_{Ga} acceptor at low temperature and from conduction band to Mg_{Ga} acceptor at elevated temperature. Thus, we concluded that the BL band we see in our sample is, in fact, the UVL band but emerging from the regions of the sample where potential fluctuations are present. We, therefore, called BL band the BL^{*} band.

We also studied the temperature dependence of the PL peak intensity at fixed excitation intensities. UVL band was observed to undergo tunable quenching (not abrupt) with an activation energy of $100 - 125\, meV$. Abrupt and tunable thermal quenching was observed for Exciton band at all excitation intensities but it was observed for BL^{*} band only at comparatively lower excitation intensities. Abrupt and tunable thermal quenching in PL bands was explained by the phenomenological model. This model assumes shallow acceptors (Mg_{Ga} in our case), shallow donors and unknown nonradiative deep donors (S) as the defects participating in the recombination of photo-generated carriers. According to the model, as the sample is illuminated at low temperature ($T < T_0$), nonradiative S centers are saturated with electrons, which results in accumulation of free electrons in the conduction band. At $T > T_0$, holes at shallow acceptors get enough thermal energy to be emitted to the valence band. Electrons at S centers efficiently recombine with the holes in the valence band. This leads to the abrupt thermal quenching of the PL. Inverse of characteristic temperature was plotted as a function of electron-hole pair generation rate for each band. From the slope of the

plot, ionization energy of the acceptor responsible for thermal quenching was obtained to be $240 - 250\ meV$ which is close to the ionization energy of $150 - 200\ meV$ of Mg_{Ga} acceptor.

Small blueshift of the BL* band with increasing temperature ($P_{exc} > 0.0002\ W/cm^2$) was explained by potential fluctuations in the sample and the giant shift ($P_{exc} \leq 0.0002\ W/cm^2$) was assumed to be observed due to the abrupt and tunable thermal quenching of intensity of BL* band along with potential fluctuations. The reason behind considering abrupt thermal quenching of the intensity of BL* band to be responsible for the giant shift of the band is the following. Critical temperature (T^*) at which the giant shift begins and the characteristic temperature (T_0) at which the quenching begins were found to be almost same. At $T < T_0$, high concentration of free electrons (due to inverse population) partially screens potential fluctuations. At $T \approx T_0$, the concentration of photogenerated free electrons abruptly drops, and GaN in these regions becomes insulating. Potential fluctuations abruptly rise and the BL* band exhibits giant red-shift in a narrow temperature range.

Finally, the effect of surface condition on the BL* band was noticed. The temperature dependence of this band depended on how long the sample was stored in vacuum and being illuminated with HecD laser. Temperature dependence of BL* and UVL peak intensity was plotted for fixed excitation intensity but at different "environmental conditions". Plots for the UVL band do not change with improving vacuum in the cryostat, but BL* band loses its abrupt thermal quenching nature after the sample was exposed to air for 25 days. However, as the sample is kept in the vacuum for prolonged period, the quenching behavior was almost restored. This observation

supports our assumption that the BL^* band comes from the different region than the UVL and exciton band. Since BL^* band is affected by the outside conditions, it was reasonable to assume that BL^* band comes from the surface region. The exact mechanism of the effect of the surface condition on the BL^* band is unknown.

References

[1] E. R. Glaser *et al.*, Phys. Rev. B **51**, 13326 (1995).
[2] U. Kaufmann, M. Kunzer, M. Maier, H. Obloh, A. Ramakrishnan, B. Santic, and P. Schlotter, Appl. Phys. Lett. **72**, 1326 (1998).
[3] B. J. Skromme and G. L. Martinez, Mater. Res. Soc. Symp. Proc. **5S1**, W9.8 (2000).
[4] M. A. Reschikov, G.-C. Yi, and B. W. Wessels, Phys. Rev. B **59**, 13176 (1999).
[5] H. Obloh, K. H. Bachem, U. Kaufmann, M. Kunzer, M. Maier, A. Ramakrishnan, and P. Schlotter, J. Cryst. Growth **195**, 270 (1998).
[6] E. Oh, H. Park, and Y. Park, Appl. Physics. Lett. **72**, 70 (1998).
[7] B. I. Shklovskii and A. L. Efros, Electronic Properties of Doped Semiconductors (Springer, Berlin, 1984), pp. 53-73 and 253-313.
[8] H. P. Gislason, B. H. Yang, and M. Linnarsson, Phys. Rev. B **47,** 9418 (1993).
[9] P. W. Yu, J. Appl. Phys. **48, 5043** (1977).
[10] A. P. Levanyuk and V. V. Osipov, Usp. Fiz. Nauk **133**, 427 (1981) [Sov. Phys. Usp. **24**, 187 (1981)].
[11] D. G. Thomas, J. J. Hopfield, and W. M. Augustyniak, Phys. Rev. **140**, A202 (1965).
[12] E. Zacks and A. Halperin, Phys. Rev. B **6**, 3072-3075 (1972).
[13] M. A. Reschikov, A. A. Kvasov, M. F. Bishop, T. McMullen, A. Usikov, V. Soukhoveev, and V. A. Dmitriev, Phys. Rev. B **84**, 075212 (2011).
[14] M. A. Reschikov, J. D. McNamara, S. Fernandez, and R. Calarco, "Tunable thermal quenching of photoluminescence in Mg-doped p-type GaN"-Phys. Rev. B **85**, 245203 (2012).
[15] M. A. Reschikov, J. D. McNamara, and F. Shahedipour-Sandvik, "Tunable thermal quenching of photoluminescence in GaN"-Phys. Status Solidi C **11**, 389-392 (2014).
[16] M. A. Reschikov and H. Morkoç, "Luminesce properties of defects in GaN"- J. Appl. Phys. **97**, 061301 (2005).
[17] O. Gelhausen, M. R. Phillips, E. M. Goldys, T. Paskova, B. Monemar, M. Strassburg, and A. Hoffmann, Mater. Res. Soc. Symp. Proc. 798, Y5.20 (2004).
[18] M. A. Reschikov, D. O. Demchenko, J. D. McNamara, S. Fernández-Garrido and R. Calarco, "Green luminescence in Mg-doped GaN"- Phys. Rev. **90**, 035207, (2014).
[19] L. Eckey, U. Von Gfug, J. Holst, A. Hoffmann, A. Kaschner, H. Siegle, C. Thomsen, B. Schineller, K. Heime, M. Heuken, O. Schön, and R. Beccard, J. Appl. Phys. **84**, 5828 (1998).
[20] B. Monemar, "Fundamental energy gap of GaN from photoluminescence excitation spectra"- Phys. Rev. B **10**, 676-681 (1974).
[21] A. G. Milnes, *Deep Impurities in semiconductors* (Wiley, New York, 1973), p. 6.
[22] D. Bimberg, M. Sondergeld, and E. Grobe, Phys. Rev. B **4**, 10 (1971).
[23] J. P. Long and V. M. Bermudez, *Phys. Rev. B.* **66**, 121308 (2002).
[24] M. Eyckeler, W. Monch, T. U. Kampen, R. Dimitrov, O. Ambacher, and M. Stutzmann, *J. Vac. Sci. Technol. B* **16**, 2224 (1998).
[25] M. A. Reshchikov, M. Foussekis, A. A. Baski, *J. Appl. Phys.* **107**, 113535 (2010).
[26] L. Kronik and Y. Shapira, *Surf. Sci. Rep.* **37**, 1, (1999).

[27] M. Foussekis, J.D. McNamara, A. A. Baski, M. A. Reshchikov, *Appl. Phys. Lett.* **101**, 082104 (2012).